universität wien

DIPLOMARBEIT

Titel der Diplomarbeit

Connecting double strand breaks and synaptonemal complex assembly in *C.elegans*

angestrebter akademischer Grad

Magistra der Naturwissenschaften (Mag. rer.nat.)

Verfasserin / Verfasser:	Christina Wegrostek
Studienrichtung/Studienzweig:	A490 Molekulare Biologie
Matrikelnummer:	a0202247
Betreuerin / Betreuer:	Dr.Verena Jantsch-Plunger

Wien, im Juni 2011

Table of Contents

Abstract:

The *C.elegans him-19* gene is required in early meiotic prophase 1. Cytological observations showed that *him-19* mutant worms are likely deficient in double strand break (DSB) induction and synaptonemal complex (SC) formation (as evidenced by SYP-1 polymerization), which can be partially rescued by artificially induced breaks by γ-irradiation. In contrast, DSB induction –the prerequisite for recombination- and synaptonemal complex assembly between chromosomes were reported to take place independently in wild-type *C.elegans* meiosis. However, the *C.elegans him-19* mutant revealed that DSBs and synaptonemal complex assembly can be connected through a new pathway and the *him-19* genetic background allowed me to investigate the role of recombination intermediates promoting or inhibiting SYP-1 polymerization. *C.elegans* double mutants affected in different steps of DSB-processing, mostly concerning the homologous recombination pathway (*mre-11, rad-51, msh-5 and zhp-3)* and chromosome movement *(sun-1*) showed restricted SYP-1 polymerization in the *him-19* deficient background. Even though artificially induced DSBs partially restore SYP-1 localization onto chromosomes in *him-19*, they do not circumvent the need of MRE-11, RAD-51 and MSH-5 for triggering SYP-1 polymerization in the absence of HIM-19. Interestingly, SYP-1 polymerized more extensively in irradiated *him-19 zhp-3* when compared to *him-19* single mutants. Thus my work uncovered a novel activity of the ZHP-3 protein in restricting SC polymerization. In contrast to enhanced SYP-1 polymerization in irradiated *him-19* mutants, homologous pairing of chromosomes was not augmented upon irradiation as assessed by FISH analyses, indicating non-homologous synapsis or SC polymerization onto individual chromosome axes.

Zusammenfassung:

Das *C.elegans him-19* Gen wurde als ein Faktor identifitziert, der in der frühen meiotischen Prophase-1 benötigt wird. Zytologische Beobachtungen zeigten, dass mutierte *him-19* Würmer wahrscheinlich fehlerhaft in der Induktion von DNS Doppelstrang-Brüchen (DSB) und im Aufbau des synaptonemalen Komplexes (gemessen an der Polymerisation von SYP-1) sind, welche teilweise durch künstlich induzierte DSBs via gamma-Betrahlung wieder hergestellt werden können. Im Gegensatz dazu wurde berichtet, dass die Induktion von DSB –die Voraussetzung für Rekombination- und der Aufbau des synaptonemalen Komplexes (SC) zwischen den Chromosomen unabhängig voneinander stattfinden in der Meiose von Wildtyp *C.elegans*. Dennoch zeigten *C.elegans him-19* Mutanten, dass DSB und Aufbau des SC in einem neuen Pfad verbunden werden können. Der genetische Hintergrund von *him-19* erlaubt mir die Rolle von Rekombinations-Zwischenprodukten in der Förderung oder Hemmung der Polymerisation von SYP-1 zu untersuchen. *C.elegans* Doppel-Mutanten, welche in verschiedenen Schritten der DSB-Prozessierung beeinträchtigt und hauptsächlich an homologer Rekombination (*mre-11, rad-51, msh-5 and zhp-3)* und Chromosomen-Bewegung *(sun-1*) beteiligt sind, zeigten eingeschränkte SYP-1-Polymerisation in einem Hintergrund mit fehlerhaftem *him-19* Gen. Auch wenn künstlich induzierte DSB teilweise die Lokalisation von SYP-1 wieder herstellen, umgehen diese nicht die Notwendigkeit von MRE-11, RAD-51 und MSH-5 um die Polymerisation von SYP-1 in der Abwesenheit von HIM-19 einzuleiten. Interressanterweise polymerisiert SYP-1 durch Betrahlung wesentlich ausgedehnter in *him-19 zhp-3* verglichen zu *him-19* Mutanten. Folglich deckte meine Arbeit eine neue Aktivität des ZHP-3 Proteins in der Beschränkung der SC-Polymerisation auf. Im Gegensatz zu der verbesserten Polymerisation von SYP-1 in bestrahlten *him-19* Mutanten zeigten FISH Analysen, dass die homologe Chromosomen-Paarung durch Bestrahlung nicht erhöht werden konnte , was wiederum auf nicht-homologe Synapse oder SC Polymerisation auf individuellen Chromosomenachsen hinweist.

Introduction:

Meiosis:

Diploid sexually reproducing organisms contain one maternal and one paternal set of chromosomes. These organisms- including mammals- generate haploid gametes for sexual reproduction by using a specialized cell division, named meiosis (Roeder 1997; Petronczki, Siomos et al. 2003). After one round of DNA replication, two consecutive rounds of nuclear divisions, called meiosis 1 and meiosis 2, take place to reduce the ploidy by half. In meiosis 1, the reductional division, pairs of homologous chromosomes are separated and in meiosis 2, the equational division, the sister chromatids are segregating into two haploid gametes. Resulting gametes of two sexes fuse after fertilization.

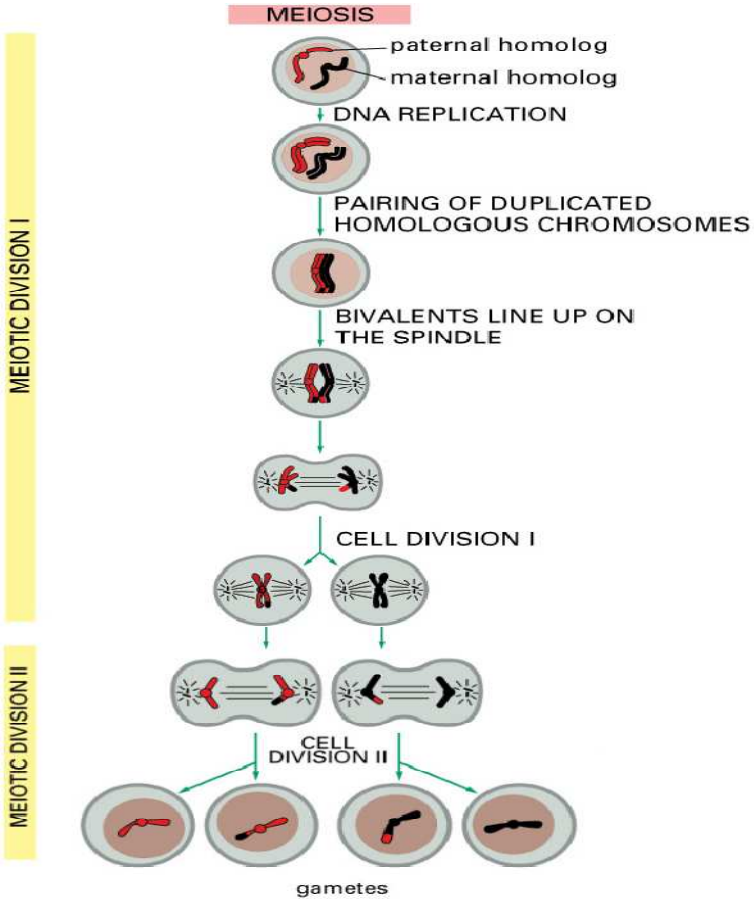

Figure 1.1 shows a schematic overview of meiosis representing the important aspect of dividing the chromosome set by half and newly assort the genetic material (Figure taken from *Alberts et al., Molecular Biology of the Cell, Fourth Edition. Garland Science, New York)*.

To secure genetic heterogeneity, reciprocal recombination events take place between homologs to assort sets of parental alleles newly during the first meiotic division (Cromie and Smith 2007). Therefore at least one crossover (CO) is established between two homologous chromosomes. COs additionally ensure proper chromosome alignment on the metaphase plate needed for faithful segregation at anaphase-1. The Induction of meiotic DNA double strand brakes (DSBs) at the onset of meiotic prophase-1 and processing into crossovers occurs in a highly spatiotemporal-regulated manner and involves many different key players conserved from human to mice, worms and flies (Petronczki, Siomos et al. 2003; Gerton and Hawley 2005). Because this work will focus on these essential early events in meiosis 1, a short overview of meiotic prophase-1 stages is given first. Afterwards chromosomal recombination events and involved proteins being relevant for this thesis are described.

Meiotic Prophase-1:

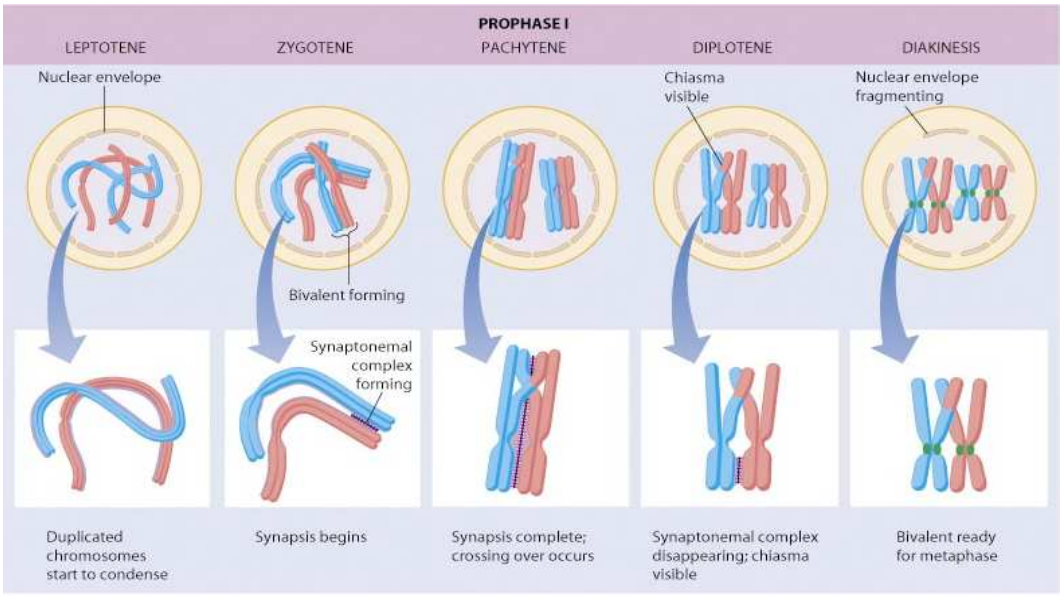

Figure 1.2 shows a cartoon of the five stages of meiotic prophase-1, which are described more detailed in the following text. (Figure © 2005 Pearson Education)

At the leptotene stage the duplicated chromosomes condense and arrange very close to each other (Bhalla and Dernburg 2008). This conformation facilitates finding the homologous partner and chromosomes can be seen presynaptically aligned at a distance of ~400nm (Zickler 2006). When the correct partners have found each other, bivalents start to form and are stabilized through building up a proteinaceous scaffold, called the synaptonemal complex (SC) in zygotene (Colaiacovo 2006). In parallel, recombination events take place between parallel assorted chromosomes (Petronczki, Siomos et al. 2003). In meiosis the prevalent DNA repair mechanism employed is homologous recombination (for details, see below). A subset of breaks uses the parental homolog as a repair template; this leads to the establishment of a physical linkage between those two chromosomes. The SC is fully formed linking the homologs in pachytene and chromosomes are cytologically spaced by ~100nms (Zickler 1999). In this context COs are formed (Neale and Keeney 2006). At the diplotene stage the SC disassembles from chromosomes and crossovers are cytologically visible as chiasmata that secure the linkage of chromosomes until the first meiotic division (Petronczki, Siomos et al. 2003). Chromosomes condense again and appear as bivalent at diakinesis ready for the following segregation.

Meiotic Recombination:

The initiation of programmed meiotic DSBs (Figure 1.3/1) at the onset of meiotic prophase-1 is the prerequisite for recombination; this is done by the endonuclease Spo11 representing a topoisomerase of type II conserved among eukaryotes. This meiosis-specific enzyme is involved in cleavage of double-stranded DNA (dsDNA) through a transesterase reaction and remains covalently linked to the 5'-end of the DNA (Bergerat, de Massy et al. 1997; Keeney, Giroux et al. 1997; Keeney 2001). In higher eukaryotes the conserved MRN repair complex composed of three proteins Mre11, Rad50 and Nbs1 (Xrs2 in *Saccharomyces cerevisiae*) is essential for early detection of DSBs and is required for DSB-end processing. In meiosis Mre11 is required for activating the DNA-damage checkpoint and cleaving Spo11 off the DNA 5´-ends to allow the resection of single-stranded DNA (ssDNA) for the following DNA-repair (Borde 2007). Furthermore, it has been suggested that the activity of Com1/Sae2 is essential for the MRN/MRX repair complex to remove Spo11 from the meiotic DSBs and for 5´to 3´resection of ssDNA (McKee and Kleckner 1997; Prinz, Amon et al. 1997; Penkner, Portik-Dobos et al. 2007).

Even though the exact regulation is not clear the DNA-repair complex generates 3´ssDNA overhangs (Figure 1.3/2) that load subsequently Dmc1 and/or Rad51 important for strand invasion (Shinohara, Ogawa et al. 1993; Rinaldo, Bazzicalupo et al. 2002; Alpi, Pasierbek et al. 2003; Colaiacovo, MacQueen et al. 2003). Both RecA-related proteins build nucleofilaments with the DNA overhangs and mediate strand exchange between the homologs. This process named single end invasion (SEI; see Figure 1.3/3) generates a D-loop that can either lead to a crossing-over or a non-crossover dependent on the stability of the D-loop structure (Neale and Keeney 2006). Here the difference between mitotic and meiotic DNA-repair arises: In mitotic cells the sister chromatid is used as a template for repairing DNA while in contrast meiotic cells achieve DNA-repair using the homologous non-sister chromosomes for repair templates. In the germline-specific DNA-repair mechanism DNA-synthesis leads to an extended D-loop (Figure 1.3/4) and the second free 5´-DSB-end is re-annealed (second end capture; see Figure 1.3/5) resulting in two double Holliday junctions (dHJ; see Figure 1.3/6). Dependent on the dHJ-resolution mechanism employed the recombination intermediates yield a crossover or a non-crossover (Figure 1.3/7). The conserved MutS family member, the meiotically expressed Msh5 protein, has been suggested to play a role in the conversion of recombination intermediates into crossover and subsequently in chiasmata formation (Kelly, Dernburg et al. 2000; Borner, Kleckner et al. 2004; Snowden, Acharya et al. 2004; Di Giacomo, Barchi et al. 2005; Snowden, Shim et al. 2008). Consistently, alterations in human Msh5 have been reported to be associated with premature ovarian failure (POF) by (Mandon-Pepin, Touraine et al. 2008). Even its biochemical function has not yet been elucidated, the Msh4/5 complex has been proposed to play a role in supporting the development of dHJs into crossovers and therefore regulating directly crossover outcome.

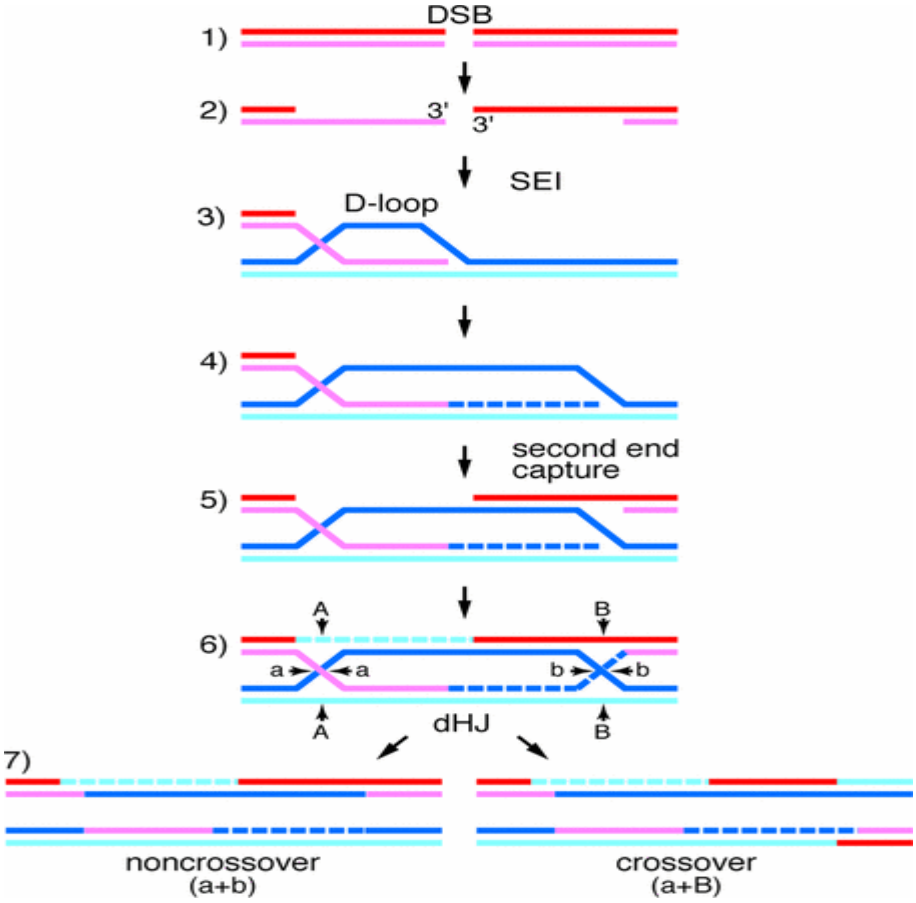

Figure 1.3 Schematic illustration (Szostak, Orr-Weaver et al. 1983) shows the key events of meiotic recombination leading to a crossover (later processed into chiasmata). To facilitate understanding only one chromatid of each homologous chromosome is drawn (one in red, the homolog in blue).

As outlined above the important aspect of meiotic DNA DSB-repair is the use of the complementary sequence from the homologous chromosome instead of the sister-chromatid. Therefore homologous parental chromosomes have to arrange side-by-side (presynaptic alignment) at the onset of meiotic prophase I to allow homologous parental chromosomes to pair and exchange corresponding sequences. Different eukaryotes undergoing meiosis arrange their chromosomes in special structures possibly to aid the chromosomes find their correct partner. This spatial reorganization of chromosomes within the nucleus appears as telomeres cluster at the nuclear periphery, referred to as the bouquet stage. In most eukaryotes this is accompanied by vigorous chromosome movement (Zickler and Kleckner 1998; Scherthan 2007). This dynamic behavior of chromosomes seems to play a crucial role in early meiotic processes, such as homologous pairing of chromosomes and early recombination events. Mechanisms regulating and

moving chromosomes during nuclear rearrangements are not fully understood yet, but recent studies discovered an active search mechanism. It seems to aid chromosomes find their homologous partner during this period (Fridkin, Penkner et al. 2008). It has been reported that the transmembrane proteins (SUN-1- and KASH-domain proteins) connect the nuclear lamina with the cytoskeletal network (actin and/or microtubules) through the nuclear envelope. Recent studies indicated that kinetic forces of the cytoplasm drive SUN-mediated chromosome-movement along the nuclear periphery, representing a highly dynamic process essential in promoting homologous pairing and discouraging wrong (non-homologous) interactions (Penkner, Fridkin et al. 2009; Sato, Isaac et al. 2009; Baudrimont, Penkner et al. 2010). Following intimate association -close, stable homolog juxtaposition (CHJP) of homologs is stabilized through pairing interactions (Peoples-Holst and Burgess 2005). To establish synapsis, the synaptonemal complex (SC) forms a physical link between the chromosomes in a zipper-like proteinaceous structure (see Figure 1.4) {reviewed by (Zickler 1999; Page and Hawley 2004)}. For a long time it was believed that synapsis takes place between homologous chromosomes only in a DSB-dependent manner as reported for *Saccharomyces cerevisiae, Arabidopsis thaliana*, *mus musculus* and human (Peoples-Holst and Burgess 2005; Zickler 2006). In contrast, additionally DSB-independent mechanisms triggering homologous alignment and initial SC-assembly were described in *Drosophila m.* (McKim, Green-Marroquin et al. 1998) and *C.elegans* (Dernburg, McDonald et al. 1998). The occurrence, structure and function of the synaptonemal complex are conserved among sexual reproducing organisms.

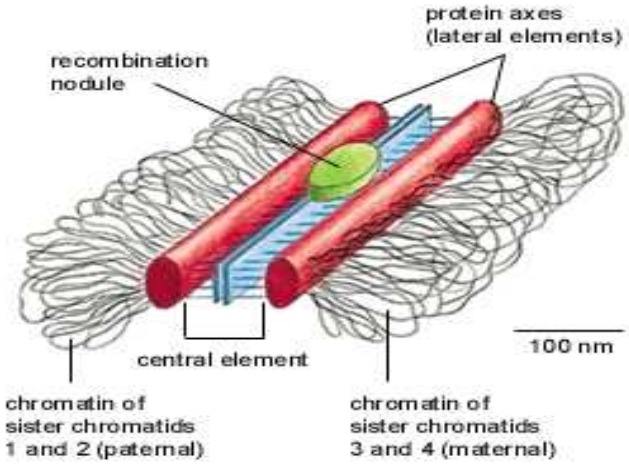

Figure 1.4 Schematic drawing of the synaptonemal complex formed between homolog chromosomes (Copyright © Alberts B, Bray D, Lewis J, et al.; New York: Garland Science; 1994). The

lateral elements are aligned along the chromatin-loops (red) and the central elements (blue) connecting them in a zipper-like structure.

In late pachytene the SC is fully formed as evidenced by parallel chromatin-tracks detectable with DAPI-staining (4',6-diamidino-2-phenylindole). After SC disassembly in diplotene, chiasmata are maintained by chromosome cohesion until the first meiotic division. At the diakinesis stage the connected chromosomes are visualized as bivalents representing homologously paired and partially newly assorted chromosomes. A more detailed discussion of genes/proteins involved in synapsis or recombination being relevant for this work will be given at the end of the introduction.

It is a fact that defects of any meiotic event –especially in meiotic prophase I- might affect correct meiotic chromosome segregation leading to aneuploidy, which is the most common chromosome abnormality in humans (Hassold and Hunt 2001; Hassold, Hall et al. 2007). Aneuploidy has been reported to be the leading genetic cause of mental retardation, miscarriage and congenital birth defects, taking place in at least 5% of pregnancies. Studies on mechanistic details of meiosis in model organisms might contribute to our understanding of risk factors for human aneuploidy.

Caenorhabditis elegans Meiotic Prophase-1:

The transparent soil nematode *Caenorhabditis elegans,* a well known and easy cultivable model organism, was used for the cytological studies of meiotic prophase-1 events in this thesis. This diploid eukaryote containing 6 chromosome-pairs is about 1mm long as an adult animal. Wild-type worms (N2 Bristol) are normally self-reproducing hermaphrodites with five pairs of autosomes and one pair of sex chromosomes (genotype X/X). In parallel a low percentage (about 0,05%) of males with one sex-chromosome (genotype X/O) is represented in the progeny arisen through X chromosome non-disjunction. The resulting ability of measuring correct chromosome segregation by a *high incidence of males* in the progeny (*him*-phenotype) facilitates detection of mutations affecting meiotic processes essential for accurate chromosome segregation. Moreover, the spatiotemporal progression and the distinct stages of meiotic prophase-1 are observable in dissected *C.elegans* gonads. Since this nematode was used the first time to analyze development and function of the nervous system (Brenner 1974) the *C.elegans* community developed a plethora of online information resources and tools (Antoshechkin and Sternberg 2007).

Additionally, different genomic centers, institutes or companies store and distribute a broad range of *C.elegans* mutant strains**.** Given all that advantages, from its biological simplicity to its transparency and to its high content of cells actively undergoing meiosis, this worm becomes an amenable tool in meiosis research.

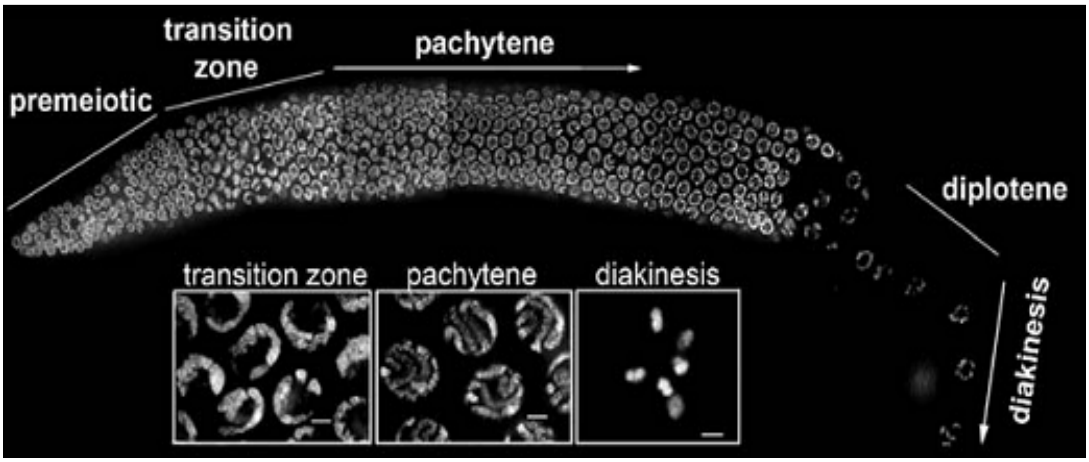

Figure 1.5 displays a dissected gonad of wild-type (N2) *C.elegans*. The distinct stages of meiotic prophase-1 nuclei are shown. Chromatin is visualized through DAPI-staining (Colaiacovo 2006).

The distal part of the *C.elegans* wild-type gonads, the premeiotic zone, consists exclusively of mitotic cells. Interphase cells enter transition zone (leptotene/zygotene) in *C.elegans* by DNA double strand break (DSB)-independent mechanisms leading to chromosome reorganization and in parallel SPO-11-dependend DSBs induce recombination (Dernburg, McDonald et al. 1998; Neale and Keeney 2006). In the transition zone (TZ) in wild-type gonads the chromatin is concentrated to one side of the nucleus adopting a half-moon shaped appearance (see Figure 1.5). In TZ, one end of each chromosome co-localizes with the nuclear envelope (NE) where the NE protein MTF-1/SUN-1 is locally enriched (Penkner, Tang et al. 2007; Fridkin, Penkner et al. 2008; Sato, Isaac et al. 2009). The interaction of the SUN-domain of MTF-1/SUN-1 protein with a KASH-domain protein connects chromosomes through the nuclear envelope to the kinetic forces of the cytoplasm to perform an active movement of the chromosomes promoting homologous and preventing non-homologous associations. When the correct partner is found, the *cis*-acting chromosomal sites adjacent to the nuclear envelope, named homolog recognition regions (HRRs) or pairing centers (PCs), stabilize pairing interactions independent of synapsis and moreover promote synapsis per se (MacQueen, Phillips et al. 2005). The

proteins (HTP-1/-2/-3, HIM-3 and REC-8) start to load onto chromosomes at transition zone respectively {reviewed by (Colaiacovo 2006)}. These axis-associated elements of SC aligning along the axes of chromosomes are a prerequisite for proper polymerization of the synaptonemal central elements. The axial element protein HTP-3 has been shown to load onto chromosome axes prior and independent of REC-8 and HIM-3 but it is essential in recruiting these axial elements to meiotic chromosomes (Goodyer, Kaitna et al. 2008; Severson, Ling et al. 2009). The cohesin kleisin family proteins REC-8, COH-3/-4 are required for cohesion of homologs until the first meiotic division and for sister-chromatid cohesion (SCC) until the second meiotic division (Pasierbek, Jantsch et al. 2001; Severson, Ling et al. 2009). Moreover REC-8 is critical for subsequent chromosomal association of HIM-3 which continues to localize onto chromosome axes until metaphase I (Zetka, Kawasaki et al. 1999; Pasierbek, Jantsch et al. 2001; Couteau, Nabeshima et al. 2004; Nabeshima, Villeneuve et al. 2004). Beside its requirement for synapsis, cytological analysis reported HIM-3 to play a role in early pairing stabilization and crossover formation. Two additionally proteins HTP-1 and HTP-2, which play a role in licensing the assembly of the synaptonemal central elements, localize along chromosome axes at TZ (Couteau and Zetka 2005; Martinez-Perez and Villeneuve 2005). At early pachytene the central element proteins SYP-1 and SYP-2 assemble between chromosome axes to form a physical link between the homologs in a zipper-like structure (MacQueen, Colaiacovo et al. 2002; Colaiacovo, MacQueen et al. 2003). Recent studies revealed two novel structural and regulatory components of the SC SYP-3 and SYP-4 required for proper synapsis (Smolikov, Eizinger et al. 2007; Smolikov, Schild-Prufert et al. 2009). SYP-1, SYP-2 and SYP-3 are dependent on each other for proper assembly onto chromosomes, while SYP-4 is essential for the correct localization of all three proteins. In late pachytene the SC is fully formed detectable by parallel chromatin-tracks dispersed through pachytene nuclei (see Figure 1.5). In the context of completed synapsis the axial-associated elements HTP-3, HIM-3 and REC-8 are referred to as lateral elements. After SC disassembles in diplotene HIM-3 and REC-8 continue to localize along chromosome axes ensuring chromosome arm cohesion until the first meiotic division (Pasierbek, Jantsch et al. 2001; Nabeshima, Villeneuve et al. 2005). In parallel, chiasmata (resulting from recombination event) contribute to cohesion of homolog chromosomes until the first meiotic division after SC disassembly in diplotene coupling meiotic recombination with chromosome segregation. At the onset of diakinesis chromatin condenses and becomes visible as six bivalents indicating six pairs of homologous chromosomes (see Figure 1.5).

The role of *him-19* in *C.elegans* meiosis:

During my diploma thesis work I used the mutant allele *him-19(jf6),* isolated by an ethane methyl sulfonate (EMS) mutagenesis screen performed with the TY2441 *C.elegans* strain (Tang, Machacek et al. 2010). The high occurrence of males in the progeny of mutant hermaphrodites indicates a defect in X-chromosomal disjunction. As *xol-1* is expressed in TY2441 males only, the tagged *xol-1*:GFP (Green Fluorescence Protein) transgene was used as a tool in a screen for mutant hermaphrodites being defective in chromosome segregation. One recessive allele named *him-19(jf6)* was found, bearing a G->A transition in the 6th intron at the splice acceptor site. At least three different splice variants of the *jf6* allele exist leading either to a premature STOP or a transcript missing exon 7 (for details see Materials and Methods). As the name suggests, the mutated *him-19* (high incidence of males) gene leads to a high frequency of males in the progeny (~19%) and an increase in embryonic lethality. In contrast, wild-type (N2) worms display 0,2% males in the progeny (Hodgkin, Horvitz et al. 1979). Furthermore, the *him-19(jf6)* phenotype aggravates in a female-specific age-dependent manner. In *him-19(jf6)* the hatch rate of laid eggs averages 24% observed over the first three days of fertility (day1~51%; day2 ~17%; day3 ~4%). Essential meiotic prophase-1 events, such as homologous chromosome pairing (evaluated by FISH) and synapsis (evaluated by Immunofluorescence against SYP-1), are affected in those mutants (Tang, Machacek et al. 2010). Aged *him-19(jf6)* mutant worms display no detectable transition zone (leptotene/zygotene) and a high incidence of univalents at diakinesis.

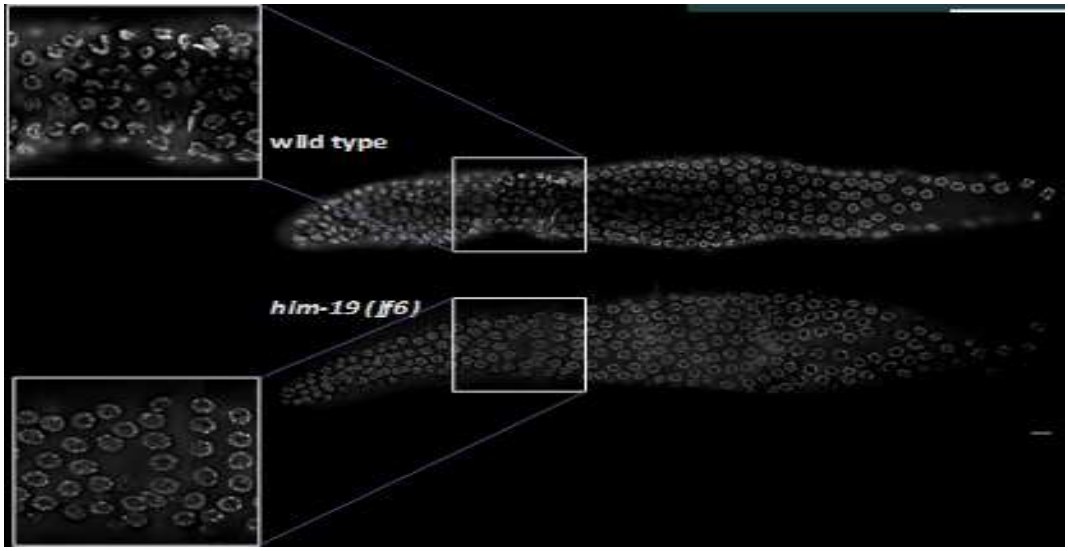

Figure 1.6 (Tang, Machacek et al. 2010) demonstrates wild-type and *him-19(jf6)* mutant gonads with DAPI-stained nuclei taken with a fluorescence microscope at a magnification of 63x1 in oil; scale bar represents 5µm. In the two squares transition zones are represented enlarged for a better visualization.

The figure above shows differences in nuclei morphology between wild-type and *him-19(jf6)* mutant gonads. The reorganization of chromatin is impaired in the mutant background, concomitant with the absence of a transition zone where the homologous chromosome search is hypothesized to proceed. Cytological investigations showed that the axial elements HIM-3 and HTP-3 localize onto chromosomes in a wild-type manner indicating that meiosis is initiated normally, but the pattern of SYP-1 loading is restricted when compared to the wild-type background. Because FISH analysis revealed high levels of non-homologous chromosome pairing in *him-19(jf6)* gonads, residual observed synapsis was suggested to occur between non-homologous partners.

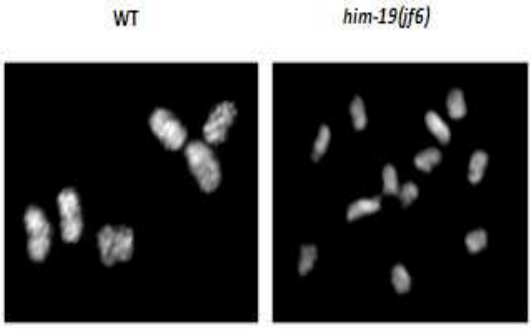

Figure 1.7 (Tang, Machacek et al. 2010) represents 6 bivalents in wild-type diakinesis in contrast to 12 univalents occurring in diakinesis of *him-19(jf6)* mutant gonads.

Always 6 DAPI signals are detectable at diakinesis in wild-type animals (Figure 1.7). In the background of 1 day old mutant *him-19(jf6)* worms, 6 to 9 signals and in 2 day old mutants 11 to 12 signals can be detected. These findings confirm the observation of an aggravation of the mutant *him-19(jf6)* phenotype over the reproductive period.

Previous studies revealed DSB-independent mechanisms promoting synaptonemal complex assembly in *C.elegans* meiotic prophase-1 (Dernburg, McDonald et al. 1998; MacQueen, Colaiacovo et al. 2002; MacQueen, Phillips et al. 2005). Polymerization of the central synaptonemal complex element SYP-1 is restricted in *him-19* mutant gonads (Tang, Machacek et al. 2010). Furthermore aged gonads are likely deficient in meiotic DSB-induction or processing. Chromosomes are not properly paired and synapsis is not as extensive as in wild-type, and if it takes place it is built up between non-homologous chromosomes. But interestingly, artificial induced DSBs via γ-irradiation partially restore SYP-1 polymerization while homologous pairing is not improved (a fact shown during my diploma thesis work). This in turn indicates a DSB-dependent pathway to promote polymerization of SC components as proposed for the *C.elegans cra-1* mutant (Smolikov, Schild-Prufert et al. 2008). Similarly in the *spo-11 cra-1* double mutant gamma irradiation elicits SC polymerization.

C.elegans mutant genes relevant for this work:

mre-11 (=yeast MRE recombination/repair homolog):

In cytological investigations of *C.elegans mre-11* mutant germ lines no RAD-51 foci were observed suggesting the requirement of MRE-11 in DSB induction or RAD-51 loading (Alpi, Pasierbek et al. 2003). These results were strengthened through studies of *mre-11 rad-51* double mutant germ-lines. The occurrence of properly condensed univalents at diakinesis indicates that DSBs were not formed and supports the requirement of MRE-11 for meiotic DSB-induction (Rinaldo, Bazzicalupo et al. 2002). Additionally, further analysis of *C.elegans mre-11* null mutants reported no cytological detectable recombination events, as evidenced by the lack of chiasmata (Chin and Villeneuve 2001), which is a consequence of defective DSB induction. Moreover, fragmented chromatin and decreasing progeny-survival after y-irradiation indicated a role of MRE-11 in the repair-pathway of radiation-induced DSBs. The meiotic G_2 DNA-damage checkpoint was shown not to be affected in

mre-11 deficient worms. These findings suggested dual functions for MRE-11 in meiotic recombination namely in DSB-induction as well as in DSB-repair in the nematode.

rad-51 (=RADiation sensitivity abnormal/yeast RAD-related):

Studies of *C.elegans* meiotic prophase 1 showed that the conserved RAD-51 protein localizes to meiotic (SPO-11 induced) DSBs (Rinaldo, Bazzicalupo et al. 2002; Alpi, Pasierbek et al. 2003) and is essential in DSB processing into crossovers [for review see (Masson and West 2001)]. Cytological observations revealed that in *C.elegans* RAD-51 associations to wild-type chromosomes start at transition zone and ~0-11 distinct RAD-51 foci per nucleus are scored which are gone in late pachytene. Mutant *rad-51* (RNAi and null mutation) worms displayed wild-type gonad morphology. But as a consequence of unrepaired DSBs, diakinesis nuclei showed uncondensed chromatin and chromosome fragmentation instead of the six bivalents, observed in the wild-type. Additionally epistasis experiments placed *C.elegans* RAD-51 clearly downstream of the DSB-induction proteins SPO-11 and MRE-11 substantiating its role in the invading step of ssDNA-ends.

msh-5 (=MSH (MutS Homolog) family):

The human meiosis-specific heterodimeric hMSH4/hMSH5 (HIM-14/MSH-5 in *C.elegans*) complex was shown to bind uniquely to Holliday Junctions (Snowden, Acharya et al. 2004). Binding of hMSH4/hMSH5 to a HJ induces ADP→ATP exchange triggered by the HJ. The protein complex binds ATP; this in turn provokes the formation of a sliding-clamp around the two homologous duplex DNA arms. Dissociation of the hMSH4/hMSH5 sliding-clamp from the dHJs crossover region allows additional hMSH4/hMSH5 binding onto HJs. Moreover, the interaction of several components of the human meiotic DNA-repair machinery with the complex was demonstrated (Snowden, Shim et al. 2008). The authors concluded that hMSH4/hMSH5 supports meiotic CO-repair by the formation of sliding-clamps around the two homologous duplex DNA molecules.

Consistently, in *C. elegans* meiosis the conserved MSH-5 protein (together with HIM-14) was reported to play a crucial role in stabilizing recombination-intermediates during homologous recombination (Kelly, Dernburg et al. 2000). *C.elegans msh-5* mutants are deficient of crossovers and achiasmate, but intact univalent chromosomes were observed

in diakinesis nuclei. These findings indicated MSH-5 as a factor needed for crossover formation, but meiotic DSBs seemed to be repaired via alternative DNA-repair pathways in worms lacking MSH-5. Further studies revealed that MSH-5 rather stabilizes crossover than non-crossover intermediates (Rinaldo, Bazzicalupo et al. 2002). Moreover, a putative role of MSH-5 in meiotic progression during meiotic prophase I was proposed. Carlton et al showed that achiasmatic chromosomes trigger a cell cycle checkpoint. The triggered cell cycle delay seems to depend on MSH-5 (Carlton, Farruggio et al. 2006).

zhp-3 (=Zip (yeast meiotic zipper) Homologous Protein):

C.elegans ZHP-3 localized along chromosomes during meiosis (Jantsch, Pasierbek et al. 2004). While loading of the AE and the SC are not dependent on ZHP-3, correct ZHP-3 association was shown to occur only when the SC was formed properly. Additional analyses of *zhp-3* mutant worms showed a highly dynamic localization pattern of ZHP-3 during meiotic prophase (Bhalla, Wynne et al. 2008). In early pachytene ZHP-3 started to localize along the SC and the loading pattern along the SC became asymmetrically and more restricted in late pachytene. Six ZHP-3 foci per nucleus were observed at the end of pachytene/diplotene indicating that each focus likely associates with the site of the unique CO on each chromosome. Thus ZHP-3 can be used as a marker for chiasmata between homologs in late pachytene/diplotene. Moreover, normal meiotic progression but the occurrence of univalents at diakinesis in *zhp-3* deficient nematodes placed ZHP-3 as an essential component of the meiotic recombination machinery in maturation of chiasmata.

sun-1 (=SUN (*S. pombe sad1*/*Ce*-UNC-84) domain protein):

The meiotically expressed *C.elegans* SUN-protein Matefin/SUN-1 plays a role in various different processes, such as centrosome attachment to the nuclear envelope, germ-cell development, telomere positioning and apoptosis (Tzur, Wilson et al. 2006; Fridkin, Penkner et al. 2008). Moreover, the SUN-1/KASH-bridge was shown to connect chromosome ends through the NE to microtubules in *C. elegans* in meiosis (Penkner, Tang et al. 2007; Penkner, Fridkin et al. 2009; Sato, Isaac et al. 2009). In vitro interaction of ZYG-12, the putative KASH partner of SUN-1, with the motor-protein dynein and time lapse

microscopy of SUN-1:GFP aggregates reinforce its function in chromosome motion (Malone, Misner et al. 2003; Penkner, Fridkin et al. 2009; Sato, Isaac et al. 2009; Baudrimont, Penkner et al. 2010). Kinetic forces in the cytoplasm trigger active movement of chromosomes via the SUN/KASH nuclear envelope (NE) bridges. This movement is believed to promote homologous and prevent non-homologous pairing interactions. A point mutation in the *sun-1* allele *jf18* displays non-homologous synapsis (Penkner, Tang et al. 2007). Furthermore, cytological examinations revealed that PC proteins are colocalizing with SUN-1 aggregates in the meiotic bouquet stage (=TZ) and are therefore thought to link chromosome-ends directly/indirectly to SUN-1 aggregates (Penkner, Tang et al. 2007).

Specific Aims:

The reported effect of γ-irradiation partially restoring SYP-1 polymerization shown in C.elegans *him-19* and *cra-1* mutants represents a DSB-dependent pathway that triggers SYP-1 polymerization (Smolikov, Schild-Prufert et al. 2008; Tang, Machacek et al. 2010). Moreover a requirement of proper recombination intermediate processing was reported for mediating correct SYP-1 polymerization in the absence of *cra-1*. In *cra-1* together with mutants defective in DSB-formation (*spo-11*) or repair (*mre-11, rad-51, msh-5),* SYP-1 loaded onto chromosomes in a restricted manner. The reported restoration of SYP-1 polymerization upon irradiation occurring in *cra-1* single mutants was not observed in any of the above mentioned *cra-1* double mutants. This in turn supports the requirement of DSB-formation and repair in a novel pathway promoting SC polymerization in *C.elegans* meiosis.

In my diploma thesis work I wanted to determine the extent of SYP-1 polymerization in *him-19* mutants with and without irradiation. Furthermore I wanted to investigate the role of certain recombination intermediates in promoting SYP-1 polymerization by constructing double mutants and compare SYP-1 polymerization in those to the single mutants upon irradiation. Therefore I constructed double mutants affected in different steps of DSB-processing, mostly concerning the homologous recombination pathway (*mre-11, rad-51, msh-5 and zhp-3)* and defective chromosome movement *(sun-1*) in the *him-19* deficient background. The effect of artificially induced DSBs in restoring SYP-1 polymerization in certain double mutant backgrounds might reveal a putative key player in DSB-dependent synapsis polymerization.

After it was evident that irradiation of *him-19* mutants led to enhanced SYP-1 polymerization accompanied by pairing center protein recruitment (Tang, Machacek et al. 2010) and SUN-1 aggregate formation , which even proved to be mobile (Penkner, Fridkin et al. 2009), I finally wanted to assess whether this enhanced synapsis was taking place between homologous chromosomes. To this end I scored the level of chromosome pairing in *him-19* mutants in 6 and 24 hour time intervals after irradiation throughout the meiotic time course.

Materials and methods:

Worm Strains and Culture Conditions:

For this work following genotypes were used:

		Strain number
LGI:	*him-19(jf6)/him-19(jf6) (I)*	*#379*
	him-19(tm3538)/him-19(tm3538) (I)	*#676*
	zhp-3(jf61) I/hT2 (I;III)	*#81*
	him-19(jf6)/him-19(jf6) (I); zhp-3(jf61) (I)/ hT2 (I;III)	*#656/#657*
LGIV:	*mre-11(ok179) IV/nT1 [unc-?(n754) let-?] (IV;V)*	*#368*
	msh-5(me23) IV/nT1[unc-?(n754) let-?] (IV;V)	*#754*
	rad-51(lg8701)dpy-13(e184) IV/nT1[let-?(m435)] (IV;V)	*#375*
LGV:	*mtf-1/sun-1(jf18) V/nT1 [qls51] (IV;V)*	*#189*

Only *him-19* mutant strains, bearing the *jf6* and *tm3538* alleles, were maintained homozygous. All other mutants cannot be maintained homozygous, because of the low amount of viable offspring (0-3%). Therefore these genotypes were maintained using a balancer. As wild-type reference served the N2 (Bristol) strain. Culturing of all *C.elegans* strains was carried out after standard conditions (Brenner 1974).

Mutant *him-19, zhp-3* and *mtf-1/sun-1 C. elegans* strains were generated in the laboratory of Dr. Verena Jantsch-Plunger. The *rad-51* mutant strain was kindly provided by Tony Gartner. All other nematode strains were kindly provided by the Caenorhabditis Genetics Center (CGC), funded by the NIH National Center for Research Resources (NCRR).

Genetic loci of *jf6* and *tm3538* alleles of used *him-19* mutant strains:

jf6 allele:

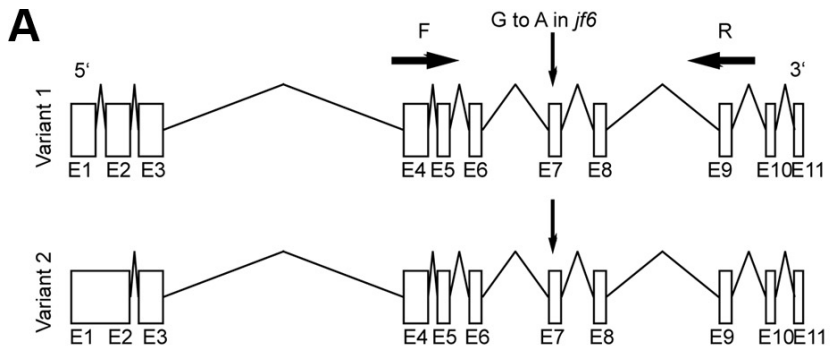

Figure 2.1 (Tang, Machacek et al. 2010); The two naturally splicing variants of *him-19(jf6)* are represented. Variant 1 has 11 exons and variant 2 has 10 exons. The single nucleotide substitution (G->A) of the *jf6* allele (arrow) is located before exon 7.

tm3538 allele:

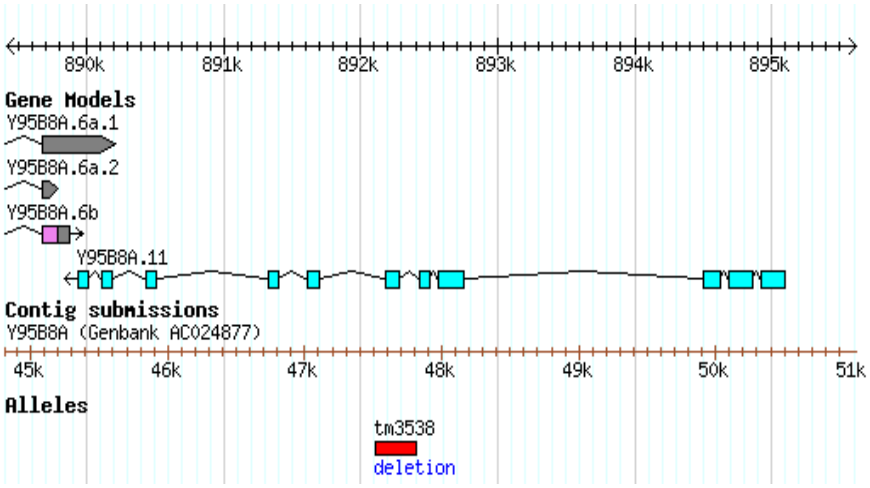

Figure 2.2 (taken from wormbase.org) illustrates genetic locus of the *tm3538* allele of *him-19* mutants. The 292bp long deletion concerns intron 5/6 and coding exon 6.

Generation of double mutants by crossing:

The crossing scheme of crossing is represented for the *him-19 msh-5* double mutant and was applied for all generated double mutants in this work.

For crossing experiments worms were selected at the larval stage 4 (L4) and seven males were mated to two hermaphrodites at 16°C. After 48 hours hermaphrodites were single plated at 20°C and transferred to another plate every day.

♀ *+ / + (I)*
msh-5 / nT1 (IV)
+ / nT1 (V)

X

him-19 / him-19 (I) ♂
+ / + (IV)
+ / + (V)

♀ \ ♂	him-19 (I) + (IV) + (V)	him-19 (I) + (IV) + (V)	him-19 (I) + (IV) + (V)	him-19 (I) + (IV) + (V)
+ (I) msh-5 (IV) nT1 (V)	him-19 / + (I) + / msh-5 (IV) +/ nT1 (V)	him-19 / + (I) + / msh-5 (IV) +/ nT1 (V)	him-19 / + (I) + / msh-5 (IV) +/ nT1 (V)	him-19 / + (I) + / msh-5 (IV) +/ nT1 (V)
+ (I) msh-5 (IV) + (V)	him-19 / + (I) + / msh-5 (IV) + / + (V)	him-19 / + (I) + / msh-5 (IV) + / + (V)	him-19 / + (I) + / msh-5 (IV) + / + (V)	him-19 / + (I) + / msh-5 (IV) + / + (V)
+ (I) nT1 (IV) + (V)	him-19 / + (I) + / nT1 (IV) + / + (V)	him-19 / + (I) + / nT1 (IV) + / + (V)	him-19 / + (I) + / nT1 (IV) + / + (V)	him-19 / + (I) + / nT1 (IV) + / + (V)
+ (I) nT1 (IV) nT1 (V)	him-19 / + (I) + / nT1 (IV) + / nT1 (V)	him-19 / + (I) + / nT1 (IV) + / nT1 (V)	him-19 / + (I) + / nT1 (IV) + / nT1 (V)	him-19 / + (I) + / nT1 (IV) + / nT1 (V)

Figure 2.3 Punnett square for the cross. Resulting F1 worms bearing the *him-19* mutation heterozygously and expressing the balancer are high-lightened in green. Genotypes of the F1-generation being heterozygous for *him-19* and *msh-5* mutations are colored in orange.

Half of the resulting F1 worms showing wild-type morphology, and therefore being heterozygous for *him-19(tm3538)* and *msh-5(me23)* mutations (orange colored in schema above). Hermaphrodites of this genotype were mated to males of the same generation showing the balancer phenotype (green colored in schema above).

♀ *him-19 / + (I)*
msh-5 / + (IV)
+ / + (V)

X

him-19 / + (I) ♂
+ / nT1 (IV)
+ / nT1 (V)

♀ \ ♂	him-19 (I) + (IV) + (V)	him-19 (I) msh-5 (IV) + (V)	+ (I) msh-5 (IV) + (V)	+ (I) + (IV) + (V)
him-19 (I) nT1 (IV) + (V)	him-19/him-19 (I) + / nT1 (IV) + / + (V)	him-19/him-19 (I) msh-5 / nT1 (IV) + / + (V)	+ / him-19 (I) msh-5 / nT1 (IV) + / + (V)	+ / him-19 (I) + / nT1 (IV) + / + (V)
him-19 (I) nT1 (IV) nT1 (V)	him-19/him-19 (I) + / nT1 (IV) + / nT1 (V)	him-19/him-19 (I) msh-5 / nT1 (IV) + / nT1 (V)	+ / him-19 (I) msh-5 / nT1 (IV) + / nT1 (V)	+ / him-19 (I) + / nT1 (IV) + / nT1 (V)
him-19 (I) + (IV) nT1 (V)	him-19/him-19 (I) + / + (IV) + / nT1 (V)	him-19/him-19 (I) msh-5 / + (IV) + / nT1 (V)	+ / him-19 (I) msh-5 / + (IV) + / nT1 (V)	+ / him-19 (I) + / + (IV) + / nT1 (V)
him-19 (I) + (IV) + (V)	him-19/him-19 (I) + / + (IV) + / + (V)	him-19/him-19 (I) msh-5 / + (IV) + / + (V)	+ / him-19 (I) msh-5 / + (IV) + / + (V)	+ / him-19 (I) + / + (IV) + / + (V)

Figure 2.4 Punnett square of the cross with the resulting genomic arrangements. Resulting F2 worms carrying the balancer are colored in green. Additionally, the desired genotype of the F2-generation homozygous for *him-19* and heterozygous for *msh-5* mutations is high-lightened with an orange background.

Resulting F2-animals carrying the balancer (expressing GFP in the pharynx; green high-lightened in schema above) were single plated at 20°C. The high occurrence of males in their progeny (F3) facilitates the screening of candidate lines being homozygous for the *tm3538* allele. This was followed by the evaluation of the designated genotype (orange background in schema above) of potential candidate line worms via PCR amplification with specific primers against *him-19(tm3538)* and *msh-5*(*me23*) genes (see following sections).

Additionally L4-hermaphrodites of potential candidate lines homozygous for both mutations were single plated and viability of the offspring was monitored (for *msh-5* not more than 3%).

DNA-preparation:

One adult worm was transferred in 8µL fresh lysis buffer and was stored for 10min at -80°C. Probes were put in a PCR-machine afterwards for running the Lysis-program: 60min at 60°C for lysis followed by 15min at 95°C (inactivation of proteinase K). Worm lysates are stored at -20°C. 1µl of the worm-lysats containing DNA were used in each detection reaction (PCR).

Evaluation of correct genotypes through PCR amplification:

Worm-lysates were used as template for PCR reaction (conditions below) with specific primers against different genes listed in following table:

Amplified gene (allele)	**Primer**	**Sequence 5´->3**	**Annealing temperature**	**Extension time**	**Amplicon**
him-19(jf6)	MJ1976 MJ1904	ATACGCAGAACGCCGTGAAC TCAAATTCTCGCCTTGTACAC	61°C	3´	wt: ~2800bp mut:~2800bp
him-19(tm3538)	VJ499 VJ500	ACGCGCCGTAAATCTACGAA ACGCCGTGAACGCTGCAAGA	54°C	1´	wt: ~800bp mut: ~600bp
mre-11(ok179)	MJ2188 MJ2189	TCATATGGATGCCGTCAACACT CAGGTTGAGAATGTCGAACATG	55°C	2´	wt: ~2200bp mut: ~600bp
rad-51(lg8701)	VJ554 VJ555	GAAAGTGTGGAGAGAAACAGAAAT CTTTCAGAGATGTTCCGGGTC	65°C	1´30´´	wt: ~1050bp mut: ~50bp
msh-5(me23)	VJ546 VJ547	GGCAAGTTGCCGGTTTGCC GATCGTCTGTCACGCCCATCC	53°C	2´30´´	wt: ~400bp mut: ~250bp
zhp-3(jf61)	MJ963 MJ964	GCCGGAAATTTTCAGTTCTGG GCCGGAAATTTTCAGTTCTGG	52°C	2´	wt: ~1900bp mut:~1800bp
mtf-1/sun-1 (jf18)	VJ593	AGGAAATCGATGATGCGGTA	59°C	40´´	wt: ~400bp

	VJ594	GGTCAAGGTCGCACGTTTAT			mut: ~400bp

For PCR amplification the following mixture was prepared and run under conditions tabled afterwards:

1 µl	DNA-template of lysated worm
2 µl	dNTP´s (à 0,25mM)
1 µl	reverse + forward Primer (1:10)
0,2 µl	Dream Taq (Fermentas)
2,5 µl	Dream Taq buffer
18,3 µl	dH_2O
25 µl	total volume 1 PCR sample

PCR-conditions:

Stage	Step	Temperature	Time	Cycles
1	1	96°C	5´	1
2	1	96°C	40´´	35
	2	(see table)	40´´	
	3	72°C	(see table)	
3	1	72°C	5´	1

Amplified DNA-samples (15µl+2,5µl 6xLoading Dye Fermentas) were loaded on a 0,1% Agarose-gel together with DNA-ladder mix (0,5µg/µl; Fermentas) as marker. The gel was

run with 80 Volt for 30 minutes in TAE. Under UV-light length of the amplicons (see primer-table) was approximately quantified through marker bands (data not shown).

Sequencing:

The three mutant alleles *him-19(jf6), mtf-1/sun-1(jf18)* and carrying single base transitions (= point mutations) had to be sequenced to evaluate correct genotypes. Therefore amplified DNA gained in PCR reactions was purified instead of analyzed on a gel.

6µl	PCR-product
0,5µl	Exo1 (E.coli; Fermentas EN0581)
1µl	SAP (=Shrimp alkaline phosphatase; Fermentas EF0511)
0,5µl	Dream Taq buffer (Fermentas)
8µl	total volume

Samples were incubated for 20min at 37°C to allow Exo1 the removal of ssDNA (Primer) and SAP the degradation of dNTP´s in PCR mixtures. After inactivation of reaction for 20min at 80°C, purified DNA probes were included in a PCR run for following sequencing. This PCR-reaction coupling amplifying and label incorporation was applied twice, each batch with one of two sequencing primers (see primer-table above).

6µl	purified DNA-sample
1µl	Big Dye (Terminator v3.1; Applied Biosystems)
2µl	one Sequencing primer (3,5:100 / see table)
1µl	ddH_2O
10µl	total volume

PCR-conditions:

Stage	Step	Temperature	Time	Cycles
1	1	96°C	2´	1
2	1	96°C	30´´	25
	2	50°C	15´´	
3	1	60°C	4´	1

Resulting samples were sent to the Institute of Botany (University of Vienna) for DNA-sequencing (short run). Transitions were verified to occur at the correct loci through sequence analysis with DNA-Strider software (Version 1.4f5, CEA France).

Irradiation Experiments:

48hours post L4-selection animals were irradiated with a dose of 5000rad (50Gy) of γ–rays using a ^{60}Co source (Gamma cell Irradiator). For the FISH assay animals were cut open to release the gonads 6 and 24 hours after γ-ray treatment. Gonads for SYP-1 Immunostaining were prepared 6hours post irradiation as described below.

Fluorescence In Situ Hybridization (FISH):

Hermaphrodites were cut 54 and 72 hours post L4 selection (larval stage L4) [6 and 24 hours post irradiation] in 1x phosphate-buffered saline (1xPBS) and the dissected gonads were fixed on a microscope slide by the addition of an equal volume of 7,4% formaldehyde. Samples were incubated under a glass cover slip for 5 minutes at room temperature and frozen in liquid nitrogen (-196°C). After removing the cover slip, the

preparations were transferred to methanol (-20°C) for 1 minute and washed 3 times in fresh 1xPBS-T (T=0,1% Tween 20) for 5 minutes at room temperature. Dehydration of the slides was carried out by 5 minutes incubations in increasing ethanol concentrations (20/50/70/90%) and following air dry after each solution.

As hybridization probe for the left arm of chromosome V the PCR-amplified 5S rDNA probe was used. During PCR amplification the 5S rDNA probe was labeled with dioxigenin-11-dUTP for direct antibody detection. After drying the amount of 150ng 5S rDNA plus 50ng sonicated salmon sperm/microscopy slide in a speed vac, the samples were resuspended in 7µl 100%formamide and 7µl hybridization-buffer (4× SSC, 20% dextransulfate) for 2,5 hours at 25°C in a shaker.

The former air dried cytological preparations were permeabelized by applying 20 µl of 1M NaSCN (Na-thiocyanat) under a plastic cover-slip for 5 min at 80°C. For hybridization the labeled DNA-probes and the prepared microscopy slides were denaturized separately for 5 minutes at 95°C. Subsequently they were incubated together for 10 min at 80°C and additionally over night at 36°C under a glass cover slip sealed with fix gum. The next day glass cover slips were removed and slides were washed in 43°C pre-warmed solutions with increasing SSC concentrations (2x/1x/0,2x/0,1x) for 5 minutes each. After block to prevent unspecific binding with 3%BSA for 20min at room temperature, hybridized labeled 5S rDNA was detected with FITC-conjugated anti-dioxigenin antibodies (1:100) for one hour at room temperature (in humidifying chamber). After 3 washes in 1xPBS-T cytological samples were mounted with Vectashield anti-fading medium (H-1000) containing 2µg/ml 4,6-diamidino-2-phenylindole (DAPI) for visualization of Chromatin. The microscopy slides were sheeted with glass cover slips and sealed with nail polish. This protocol was taken from (Pasierbek, Jantsch et al. 2001) with some modifications.

Immunostaining:

Hermaphrodites were cut on a microscope slide 54 hours post L4-selection [6 hours post irradiation] and gonads were dissected in a drop of 1xPBS. After adding a glass cover slip samples were frozen in liquid nitrogen (-196°C). Then cover slips were removed and samples fixed for 5 minutes in methanol (-20°C). For a strong fixation the slides were incubated with 3,7% formaldehyde under a plastic slip for 20 min at room temperature.

Subsequently preparations were washed 3 times in 1xPBS-T at room temperature and blocked 20 min with 3% BSA in a humidifying chamber. The primary antibody anti-SYP-1 (rabbit; #1140) was applied under a plastic cover slip o/n at 4°C in a humidifying chamber (followed by 3 washes). The secondary anti-rabbit Cy3 antibodies (goat; #1184) were incubated 3 hours at room temperature in a humid chamber (followed by 3 washes). Preparations were mounted with Vectashield anti-fading medium supplemented with 2µg/ml DAPI for visualization of chromatin. The samples were sheeted with glass cover slips and sealed with nail polish.

Microscopy and Evaluation:

Preparations were examined with a Zeiss Axioskop epifluorescence microscope. Images were recorded via a cooled charge-coupled device camera (Photometrics, Tucson, AZ) with a magnification of 63 x 1 (oil = x 1,6). For multicolor Immunostaining and FISH pictures, monochrome images were captured separately for each emission wavelength. Three-dimensional stacks of images were taken (MetaVue software; Molecular Devices, Sunnyvale, CA), deconvolved (AutoDeblur software; AutoQuant Imaging, Troy, NY), and projected (Helicon Focus software; http://helicon.com.ua/heliconfocus/).

Scoring the signals of the probe hybridized to chromosome V (5S rDNA) in the FISH-assay, gonads were divided into 7 zones of equal length starting from the distal tip and ending at the begin of diakinesis. The FISH-signals were scored as a single signal when the distance between the signals was smaller than the size of the signals themselves.

The measuring tool of Photoshop software (Adope Systems, Mountain View, CA) was applied to measure the lengths of SYP-1 stretches. At a magnification of 63 x 1 (in oil = x 1,6) 1 pixel = 66,577 nm = 0,0666 µm.

Buffers and Solutions:

Antibodies	were diluted in blocking buffer
Blocking buffer:	3%BSA (bovine serum albumin) dissolved in 1xPBS
Hybridization-buffer:	4xSSC, 20% dextransulfate
Lysis-buffer:	2,5mM $MgCl_2$, 50mM KCl, 10mM Tris, 0.45% NP-40, 0.45% Tween-20, 3µl/ml Proteinase K (20mg/ml)
PBS (Phospho-buffered saline):	
10xPBS stock-solution:	1,37M NaCl, 27mM KCl, 43mM $NaHPO_4$, 14mM KH_2PO_4
1xPBS-T:	0,1% Tween 20 diluted in 1xPBS
SSC (Saline sodium citrate):	
20xSSC stock-solution:	NaCl 175,3g, NaCitrate 88,2g bring with ddH_20 to 1L
TAE (=Tris-acetate-EDTA):	
50xTAE stock-solution:	2M Tris, 1M CH_3COONa, 50mM EDTA, adjust pH 7,4 with acetic acid

All homemade stock solutions and buffers (except alcohols) were autoclaved prior to use.

Buffers were always prepared freshly by diluting stock solutions in ddH_2O.

Results:

Phenotypic comparison of the *him-19* deletion allele *tm3538* with the originally characterized *jf6* allele

Besides the initially isolated *him-19* mutant strain bearing the *jf6* allele, a second mutant strain, *him*-19*(tm3538),* was used for experiments conducted during the course of my thesis. The *tm3538* allele carries a 292bp deletion starting at intron 5, encompassing coding exon 5 until intron 6 (for details see "Materials and methods").

I compared data from the *tm3538* allele to data on *jf6*, described in Tang et al. 2010.

To assess viability of *him-19(tm3538)* mutant worms during the reproductive period, hermaphrodites were selected at the L4 stage and single plated to allow self-fertilization. P_o animals were transferred to another plate every 24 hours and laid eggs were counted. After 24 hours residual eggs and hatched larvae (F1) were scored. Results are demonstrated in the following graph (Figure 3.1).

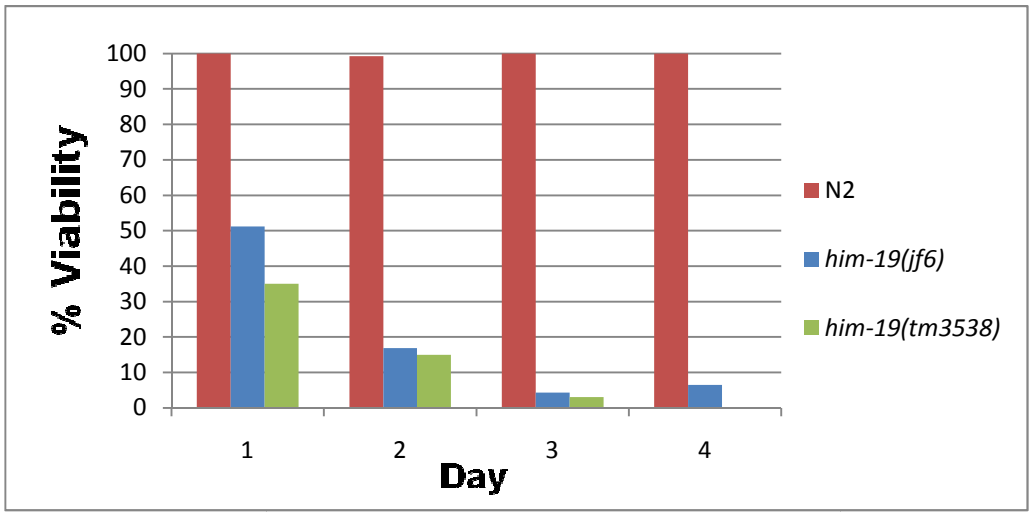

Figure 3.1 Viability (=hatch rate of eggs) over the reproductive period of self-fertilized hermaphrodite worms. Viability of both *him-19* mutant strains was opposed to wild-type background (N2). X-axis represents the four days of measurement (reproductive period) and y-axis hatch rate of eggs (or viability) in percent. Results were taken from Tang et al. 2010 and from my own counts.

As expected, the hatch rate of the wild-type was about 100%. Viability of the progeny in the *him-19(tm3538)* mutant background was comparable to that in *him-19(jf6)* over the reproductive time span (see Figure 3.1). Only on the first day the *tm3538* allele seems to have a lower hatch rate when compared to the *jf6* allele. Possibly the deletion affects *him-19* function stronger than the single point mutation.

Additionally, *him-19(tm3538)* segregates an increasing rate of males in the surviving progeny over time, as has been observed in *him-19(jf6)* (Tang, Machacek et al. 2010). Moreover, gonads of both *him-19* mutant strains showed the same morphology as they lack transition zone and univalents arise in diakinesis when chromatin was highlighted with DAPI.

SYP-1 polymerization in *him-19* mutants

With the following experiments I wanted to investigate the effect of artificially induced DSBs in restoring SYP-1 polymerization in the *him-19* deficient background. Progression of SYP-1 polymerization in *him-19* mutant germ-lines with and without artificially induced DSBs was assessed by Immunofluorescence experiments and compared to the wild-type. Therefore 2 day old worms of different genotypes were treated with y-rays and gonads were dissected 6 hours later for SYP-1 antibody staining. SYP-1 stretches were measured starting at the first cell-row where distinct and not diffuse polymerization along chromatin was observed. The progression of SYP-1 polymerization was scored over 13 cell-rows (for details see “Materials and methods”).

N2

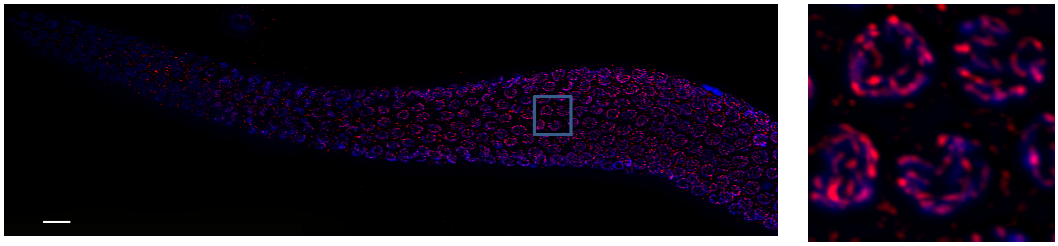

him-19(tm3538)

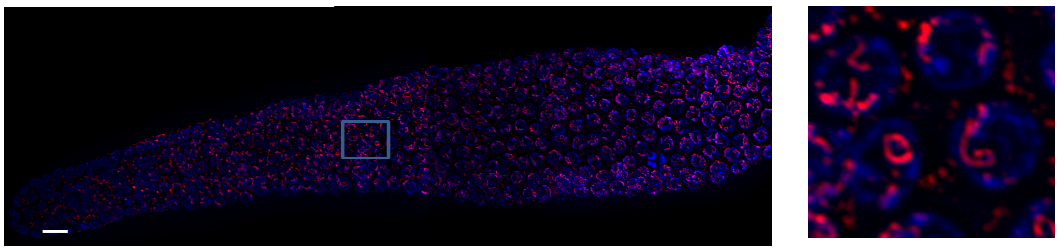

Figure 3.2 displays wild-type (N2) and *him-19(tm3538)* gonads from the distal tip until late pachytene. Pictures were taken at a magnification of 63x1 in oil. DAPI-stained chromosomes appear in blue and SYP-1 in red. Nuclei of late pachytene stage were blown up for a better visualization at the right side. Scale bars 5µm.

N2 6hrs post irradiation

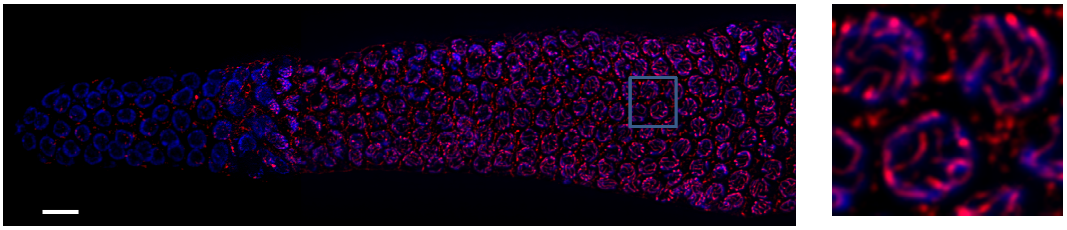

him-19(tm3538) 6hrs post irradiation

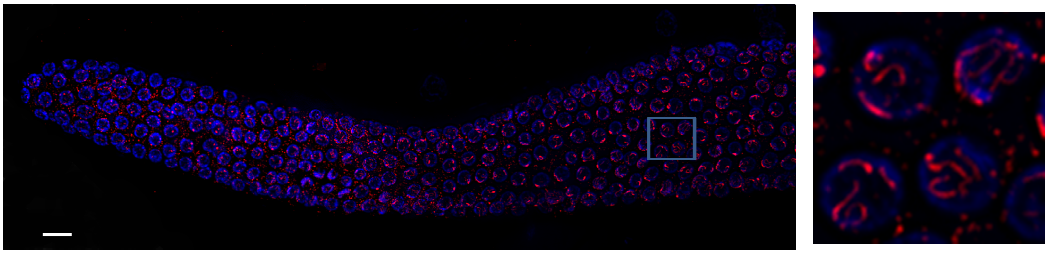

Figure 3.3 displays wild-type (N2) and *him-19(tm3538)* gonads 6 hours post irradiation from the distal tip until late pachytene. Pictures were taken at a magnification of 63x1 in oil. DAPI-stained chromosomes appear in blue and SYP-1 in red. Nuclei of late pachytene stage were blown up for a better visualization at the right side. Scale bars 5µm.

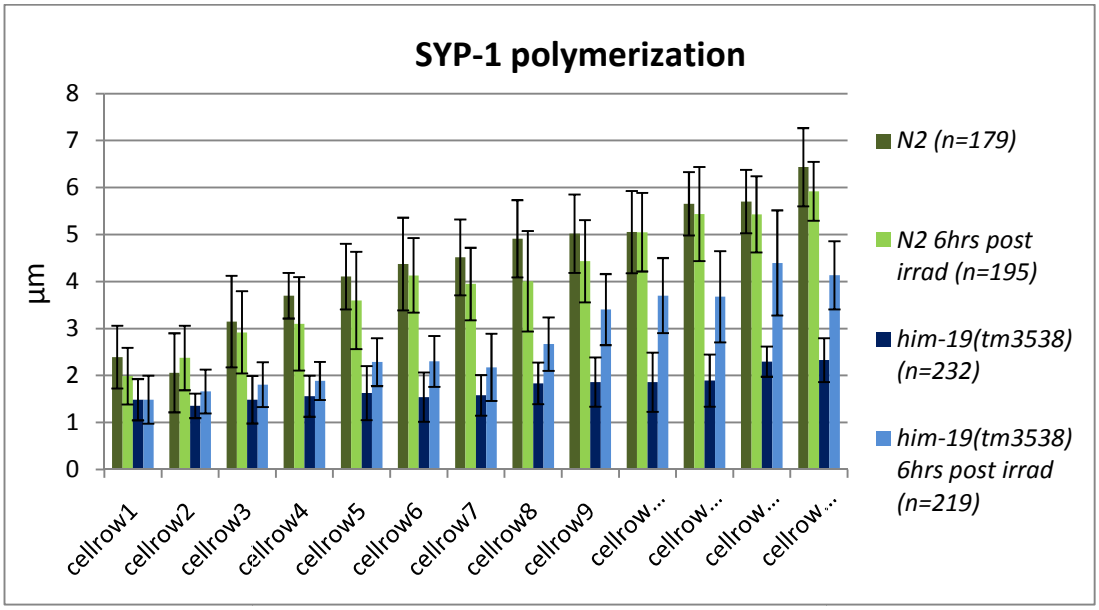

Figure 3.4 Length of SYP-1 stretches in µm (y-axis) measured over the first 13 cell-rows of polymerization (x-axis). Wild-type (N2) and *him-19(tm3538)* gonads were prepared 6 hours after y-ray treatment. Pictures gained after Immunofluorescence assays were used to measure SYP-1 stretches applying Photoshop software measure tool.

In wild-type gonads the first cell-row of distinct SYP-1 polymerization was found at the beginning of TZ, ~18-25 cell-rows after the distal tip. Scored stretches of a single nucleus averaged in length with 2,4 (±0,7) µm [see figure 3.2/3.4]. The following increase of stretch-length appeared in a continuous manner. The 13th and last measured cell-row was localized at mid-pachytene in wild-type germ-line and the calculated length of SYP-1 stretches per nucleus was 6,4 (±0,8) µm on average. For a better visualization of the differences in SYP-1 polymerization between wild-type and *him-19(tm3538)* mutant gonads, nuclei of mid and late pachytene stage were enlarged (see figure 3.2/3.3). At this point of meiotic prophase 1 the SC is fully polymerized along chromosomes in the wild type when red SYP-1 stretches fully overlap only with blue-stained chromosomes. In contrast non-synapsed chromosomes prevail in the mutant *him-19(tm3538)* background at late pachytene.

After irradiation, kinetics of SYP-1 polymerization in the wild-type shows no noteworthy difference in progression. Additionally, irradiated wild-type nuclei reveal a comparable

length at the first and the 13th cell-row averaging 2 (±0,6) µm and 5,9 (±0,6) µm respectively (see Figure 3.3/3.4).

To compare the defects in SYP-1 polymerization and its rescue upon artificially induced DSBs in both *him-19* mutant backgrounds, germ-lines were analyzed by immuno-staining against SYP-1 and the results are summarized in the following graph.

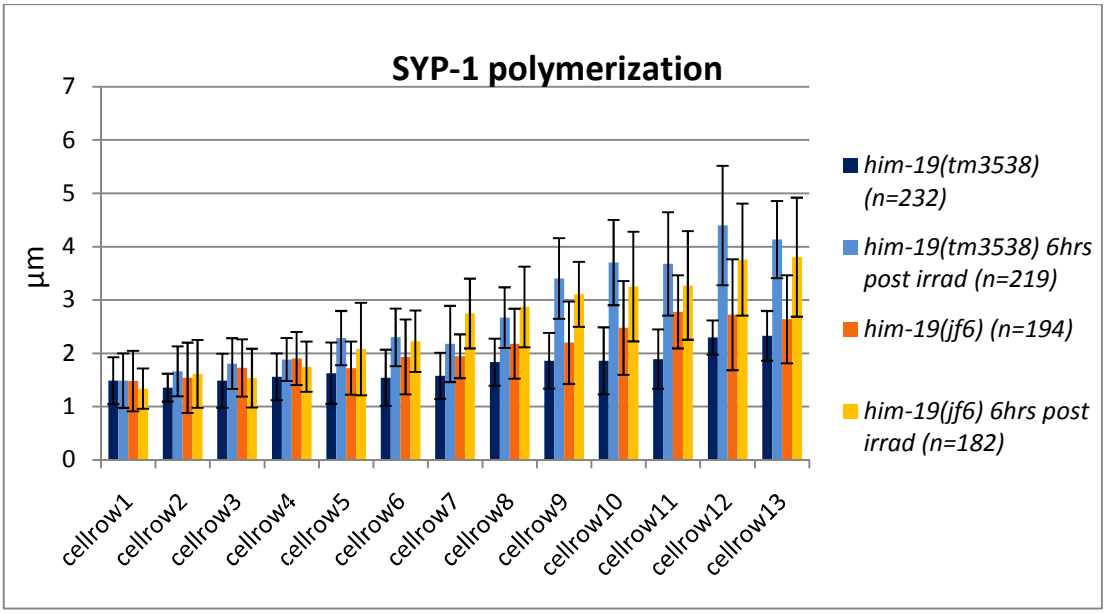

Figure 3.5 SYP-1 stretch-lengths in µm (y-axis) measured over the first 13 cell-rows of polymerization (x-axis). Gonads of *him-19(jf6)* and *him-19(tm3538)* mutants were prepared 6 hours after gamma-ray treatment. Pictures of immuno-stained gonads were taken and used to calculate SYP-1 stretches applying Photoshop software measure tool.

The first scored cell-row in *him-19* deficient germ-lines was located at the 17th-25th cell-row (when counted from the distal tip) as seen in wild-type gonads. SYP-1 polymerization in *him-19(jf6)* and *him-19(tm3538)* germ lines showed equal levels at the first calculated cell-row starting with 1,5 (±0,6) µm and 1,5 (±0,4) µm respectively (see figure 3.5). SYP-1 polymerized comparably in the *jf6* and *tm3538* alleles. However, polymerization of SYP-1 was slightly more extensive in *him-19(jf6)* worms compared to the *him-19(tm3538)* background. In the last scored cell-row I measured similar average lengths in both *him-19* deficient backgrounds: 2,3 (±0,5) µm in *tm3538* and 2,6 (±0,8) µm in *jf6.*

Radiation-treatment augmented SYP-1 polymerization in both *him-19* deficient germ lines. Meiotic nuclei in both *him-19* mutant strains started with an equal average length of

SYP-1 stretches at the first measured cell-row, consistently with the length in non-irradiated nuclei. Additionally, the time point of SYP-1 loading appeared at the 17th-25th cell-rows. Even though the progression of SYP-1 polymerization shows a more continuous loading pattern in *him-19(jf6)* worms, both *him-19* mutants display a comparable increase in SYP-1 polymerization after irradiation. At the last scored cell-row on average ~3,8 (±1,1) µm long stretches were monitored in *him-19(jf6)* nuclei, while the *him-19(tm3538)* mutation went up to a length of ~4,1 (±0,7) µm.

Taken all the results together, the two mutant *him-19* alleles showed comparable properties and defects during meiotic prophase 1. Additionally the partial rescue of SYP-1 polymerization by radiation-treatment was confirmed in both mutant *him-19* nematode strains. Subsequently both *C. elegans* mutant lines were used to generate double mutants in this work.

Investigating SYP-1 polymerization in double mutants

To assess the role of certain recombination intermediates in promoting SYP-1 polymerization, I constructed double mutants combining *him-19* deficient with mutants affected in different steps of DSB-processing, mostly concerning the homologous recombination pathway (*mre-11, rad-51, msh-5 and zhp-3)* and defective chromosome movement *(sun-1*). After constructing double mutants by crossing and evaluation of the correct genotype (see “Materials and methods”), L4 worms were selected for irradiation experiments 24 hours post L4-selection (see “Materials and methods”). Worm gonads were prepared 6 hours after y-ray treatment and SYP-1 immuno-staining was carried out (see “Materials and methods”). Pictures of gonads were used to score SYP-1 stretches in meiotic nuclei applying Photoshop software measure tool (see “Materials and methods”).

Comparing SYP-1 polymerization in *him-19* mutants with *him-19* plus a recombination mutant could uncover a possible contribution of steps of homologous recombination to SYP-1 polymerization.

Is SYP-1 polymerisation in *him-19* mutants dependent on MRE-11?

In cytological investigations of *C.elegans mre-11* mutant germ-lines no RAD-51 foci were detected and in *mre-11 rad-51* double mutants accurately condensed univalents were observed at diakinesis (Rinaldo, Bazzicalupo et al. 2002; Alpi, Pasierbek et al. 2003). Furthermore, analysis of C.elegans *mre-11* null mutants reported no cytological detectable recombination events, as evidenced by the lack of chiasmata (Chin and Villeneuve 2001). These results all together suggest the requirement of MRE-11 in meiotic DSB induction. Moreover, irradiation treatment induced fragmented chromatin and decreasing progeny-survival in *mre-11* mutant worms. This suggested an additional role of *C.elegans* MRE-11 in radiation-induced DSB-repair (Chin and Villeneuve 2001; Alpi, Pasierbek et al. 2003).

Even though gonads of *mre-11* defective worms displayed wild-type morphology with respect to occurrence of a TZ, the mutant possibly resembles *him-19* with respect to absent meiotic DSB induction (Rinaldo, Bazzicalupo et al. 2002; Tang, Machacek et al. 2010). Additionally, the proposed function of MRE-11 in radiation-induced DNA-repair might have an impact on SYP-1 polymerization upon irradiation. Therefore I studied the role of MRE-11 in polymerization of the synaptonemal central element SYP-1 in the *him-19* deficient background with and without y-irradiation treatment as described above. The lengths of SYP-1 stretches was measured and opposed to those in the *him-19(tm3538)* single mutant germ-line, see graph below.

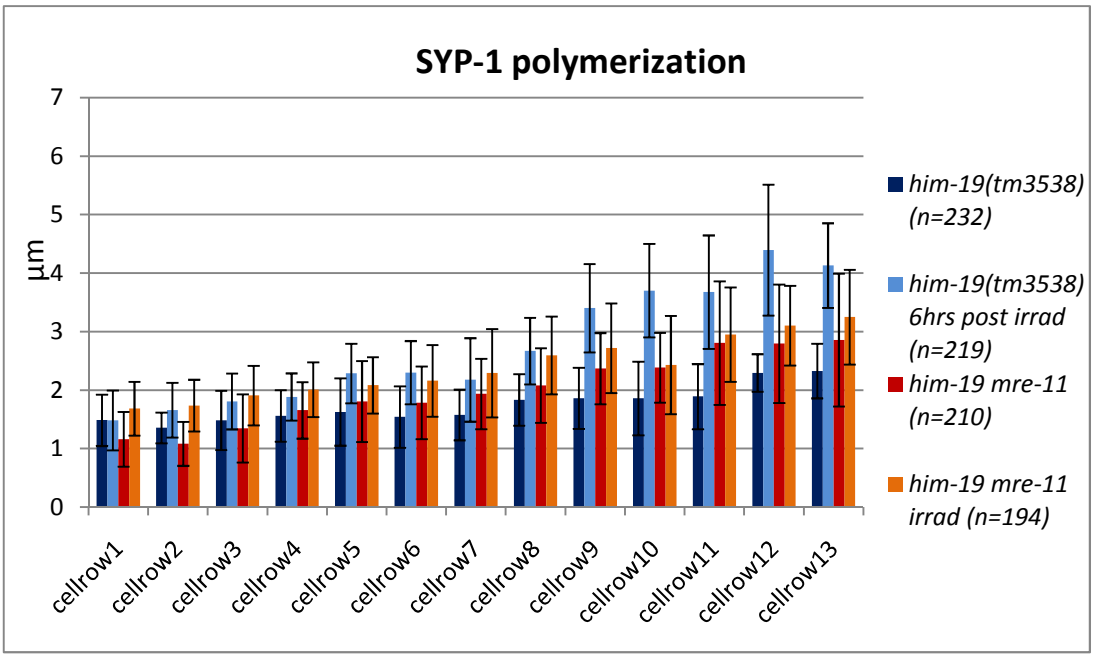

Figure 3.6 SYP-1 stretch-lengths in µm (y-axis) measured over the first 13 cell-rows after the onset of SYP-1 polymerization (x-axis). Gonads of *him-19* single and *him-19 mre-11* double mutant worms were prepared 6 hours after γ-irradiation treatment. Pictures, taken after Immunofluorescence assays, were used to score SYP-1 stretches applying Photoshop software measure tool.

Gonad morphology of *him-19 mre-11* double mutants was identical to *him-19* single mutants lacking a defined TZ with half-moon shaped nuclei. SYP-1 polymerized along chromosomes in a distinct manner at cell-row 15-25 after the distal tip comparably to wild-type and mutant *him-19* germ-lines. A slightly more extensive polymerization was observed in the *him-19 mre-11* double mutant gonads when compared to *him-19(tm3538)* [see figure 3.6]. Nevertheless, SYP-1 polymerization in the double mutant showed a similar loading pattern. In the double mutant SYP-1 stretches added up to 1,2 (±0,5) µmat the first cell-row and to 2,9 (±1,1) µm at the last cell-row compared to 1,5 (±0,4) µm and 2,3 (± 0,5) µm in the *him-19* single mutant. Only a marginal difference between averaged SYP-1 stretch lengths of the first (~0,3 µm) and the last (~0,6 µm) measured cell-row was seen compared to those observed in *him-19(tm3538)* nuclei.

Radiation-treatment led to similar SYP-1 polymerization in *him-19 mre-11* double mutants with and without irradiation. I added SYP-1 stretches at the first cell-row up to 1,7 (±0,5) µm and at the last cell-row to 3,2 (±0,8) µm compared to 1,5 (±0,5) µm and 4,1 (± 0,7) µm in the *him-19* single mutant. However, the scored SYP-1 lengths were constantly shorter over the period of measurement compared to *him-19(tm3538)* worms after irradiation.

Polymerization of SYP-1 was clearly restricted in the in *him-19 mre-11* double mutants comparable to *him-19(tm3538)* worms. However, measured SYP-1 stretch lengths of meiotic *him-19 mre-11* nuclei never reached levels monitored in the irradiated *him-19* single mutant germ-line. In contrast the SYP-1 loading pattern in irradiated *him-19 mre-11* double mutants resembled the one observed in the non-irradiated double mutant background.

Is the strand invasion step required for SYP-1 polymerisation in the *him-19* deficient background?

The conserved RAD-51 protein localizes to meiotic (SPO-11 induced) DSBs in *C.elegans* meiotic prophase 1 and is essential in DSB processing into crossovers (Rinaldo, Bazzicalupo et al. 2002; Alpi, Pasierbek et al. 2003). In *him-19(jf6)* meiosis RAD-51 was expressed properly, however it did not localize properly to chromosomes in regions where RAD-51 would be detected in the wild-type [leptotene/zygotene] (Tang, Machacek et al. 2010). The restoration of RAD-51 foci in *him-19(jf6)* cells upon irradiation suggests a defect in DSB induction in the absence of HIM-19 (Tang, Machacek et al. 2010). In *C.elegans* DSB-induction and synapsis are considered as two independent mechanisms. In contrast *him-19* mutant worms showed a partially restoration of SYP-1 polymerization upon artificially induced DSBs. The *him-19* mutant background, however allow us to ask the question whether the strand invasion step itself promotes SC polymerization.

To investigate a possible role of RAD-51 in SYP-1 polymerization in the *him-19* defective background, the constructed *him-19 rad-51* double mutant strain was analyzed in the following approach applying y-irradiation treatment followed by Immunofluorescence assays. After calculation of SYP-1 stretch lengths in meiotic nuclei the extent of SYP-1 polymerization was compared to *him-19* single mutant worm germ-lines.

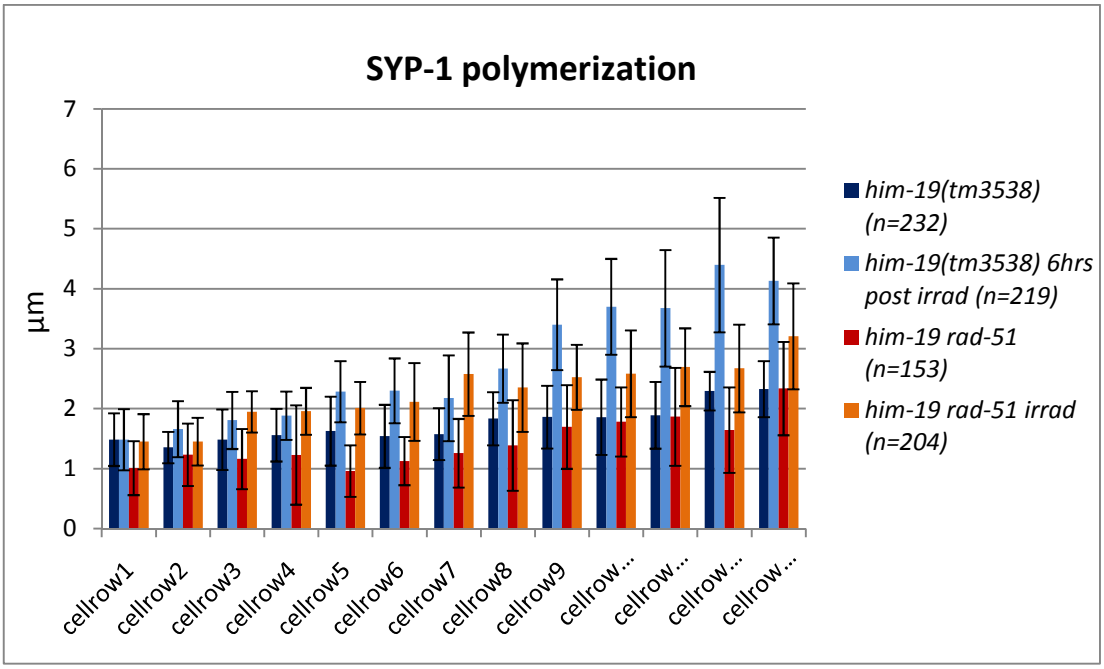

Figure 3.7 SYP-1 stretch-lengths in µm (y-axis) measured over the first 13 cell-rows after the onset of SYP-1 polymerization (x-axis). Gonads of *him-19* single and *him-19 rad-51* double mutant worms

were prepared 6 hours after irradiation. After immuno-staining, pictures of gonads were used to score SYP-1 stretches in meiotic nuclei applying Photoshop software measure tool.

Consistently to *him-19* single mutants, a distinct TZ was absent in the germ-line of *him-19 rad-51* double mutants. The first distinct SYP-1 stretches along chromosomes were seen at the 18^{th}-25^{th} cell-row and SYP-1 staining showed the same extent at the first cell-row like mutant worms only lacking *him-19*.

Measured lengths of SYP-1 stretches in *him-19 rad-51* double mutants displayed less extensive loading compared to *him-19(tm3538)* [see figure 3.7]. However, the low level of SYP-1 polymerization appeared steadily and similar to the one observed in *him-19(tm3538)* worms. While *him-19(tm3538)* cells of the last scored row exhibited SYP-1 stretches lengths of 2,3 (± 0,5) µm, I added SYP-1 stretches in the *him-19 rad-51* double mutant up to 2,3 (±0,8) µm.

Induction of DSBs by y-irradiation treatment drove SYP-1 polymerization slightly more extensive in the double mutants in contrast to the non-irradiated background. However, the localization pattern of SYP-1 progressed comparably. I calculated SYP-1 stretch lengths to 1,5 (±0,5) µm at the first cell-row and 3,2 (±0,9) µm at the last cell-row of measurement.

Summing up, SYP-1 polymerized along chromosomes in a restricted manner with and without irradiation in *him-19 rad-51* double mutant gonads comparable to *him-19(tm3538)* worms. Even though artificially induced DSBs slightly increased the extend of SYP-1 polymerization *him-19 rad-51* double mutants, the polymerization pattern observed in irradiated *him-19(tm3538)* gonads was never reached. Additionally the loading pattern of SYP-1 resembled strongly the one observed in *him-19 mre-11* double mutants.

Does SYP-1 polymerization depend on MSH-5 in the absence of HIM-19?

In *C.elegans* meiosis the conserved MSH-5 protein (together with HIM-14) was reported to play a crucial role in stabilizing recombination-intermediates (Kelly, Dernburg et al. 2000) and in triggering crossovers (Rinaldo, Bazzicalupo et al. 2002). Regulation of crossover maturation is affected in worms lacking MSH-5 and achiasmatic but intact chromosomes were observed at diakinesis. Achiasmatic chromosomes were shown to trigger a cell cycle checkpoint delaying chromatin reorganization (Carlton, Farruggio et al. 2006). MSH-5 was shown to be required for this cell cycle delay.

In this assay I wanted to study whether defective regulation of crossover maturation influences SYP-1 assembly in HIM-19 deficient animals. Therefore I created a *C.elegans* strain bearing *him-19* and *msh-5* mutations. Subsequently radiation- and immunofluorescence-experiments were carried out with generated *him-19 msh-5* double mutant gonads. Calculated SYP-1 stretch lengths of meiotic nuclei were compared to the one in the *him-19* single mutant background and are represented in following graph.

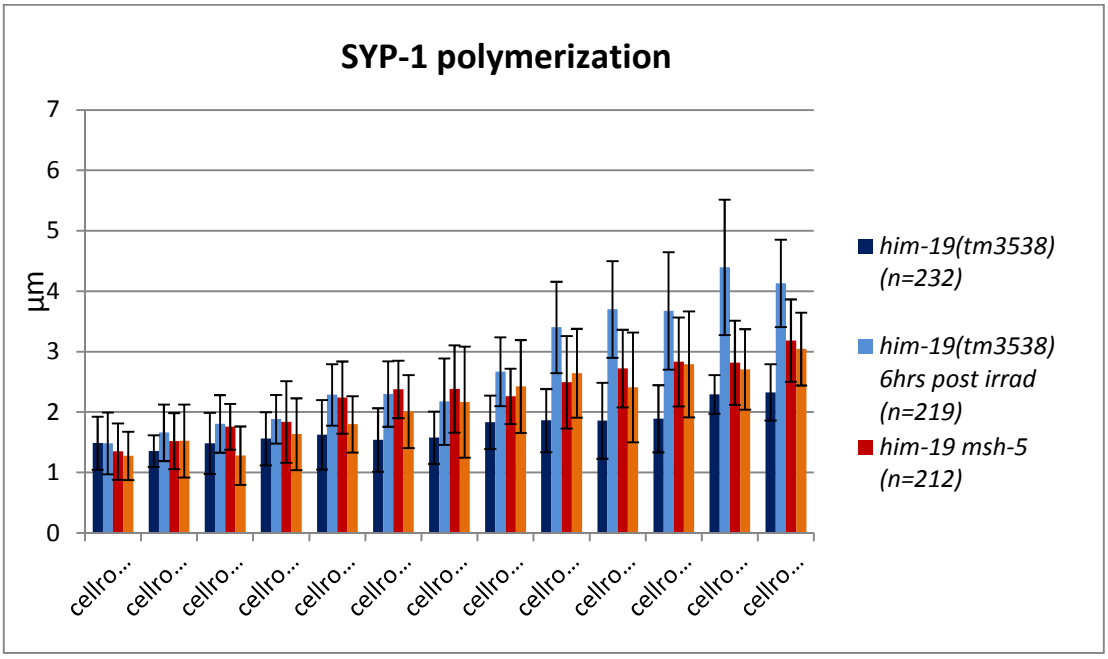

Figure 3.8 SYP-1 stretch-lengths in µm (y-axis) measured over the first 13 cell-rows upon SYP-1 polymerization (x-axis). Gonads of *him-19* single and *him-19 msh-5* double mutant worms were prepared 6 hours after gamma-irradiation treatment to apply Immunofluorescence assays. Afterwards pictures were used to calculate SYP-1 stretches applying Photoshop software measure tool.

Germ-line morphology of worms lacking HIM-19 and MSH-5 was equal to the one in *him-19(tm3538)* mutants displaying no detectable TZ. At the beginning of SYP-1 polymerization, at the 19th–25th cell-row, *him-19 msh-5* double mutants showed stretch lengths comparably to *him-19(tm3538)* nuclei. Here, I measured 1,3 (±0,5) µm in the double and 1,5 (±0,4) µm in the single mutant germ-line [see figure 3.8]. The 13th scored cell-row displayed 3,2 (±0,7) µm long stretches in *him-19 msh-5* and 2,3 (±0,5) µm long stretches in *him-19(tm3538)* gonads.

After irradiation, SYP-1 polymerized along chromosomes with a similar loading pattern like the non-irradiated *him-19 msh-5* double mutant. At the first cell-row I calculated SYP-1 stretches with 1,3 (±0,4) µm length in *him-19 msh-5* nuclei and with 1,5 (±0,5) µm length in *him-19(tm3538)* nuclei. These values were comparable to those calculated in *him-19 msh-5* gonads without artificially induced DSBs [1,3 (±0,5) µm]. The sum of SYP-1 stretch lengths of the last measured cell-row [3 (±0,6) µm] placed the extend of SYP-1 polymerization in *him-19 msh-5* germ-lines between *him-19(tm3538)* nuclei with and without irradiation [2,3 (±0,5) µm and 4,1 (± 0,7) µm respectively].

The localization pattern of SYP-1 polymerization in the double mutant with and without radiation-treatment was comparable and showed a clear restriction. Additionally, SYP-1 polymerized along chromosomes in both incidences rather with a similar restricted pattern like in *him-19(tm3538)* mutants and resembled strongly the situation in *him-19 mre-11* and *him-19 rad-51* double mutants.

Is ZHP-3 required for SYP-1 polymerization in worms defective in *him-19*?

The *C.elegans* ZHP-3 protein is an essential component of the meiotic recombination machinery for the maturation of chiasmata (Jantsch, Pasierbek et al. 2004). Additionally, ZHP-3 association with chromosomes was shown to occur only when the SC is formed properly. In further analyses of *zhp-3* mutant worms, a highly dynamic loading pattern of ZHP-3 was observed during meiotic prophase (Bhalla, Wynne et al. 2008). Moreover, ZHP-3 can be used as a marker for chiasmata between homologs in late pachytene/diplotene.

To observe a possible involvement of this regulator in crossover formation and SC-depolymerization dynamics, we compared SC polymerization in irradiated *him-19* single and *him-19 zhp-3* double mutants. The irradiation- and immunofluorescence-assays were carried out with *him-19 zhp-3* double mutant worms and the results of SYP-1 measurement are demonstrated in the following MSexel graph.

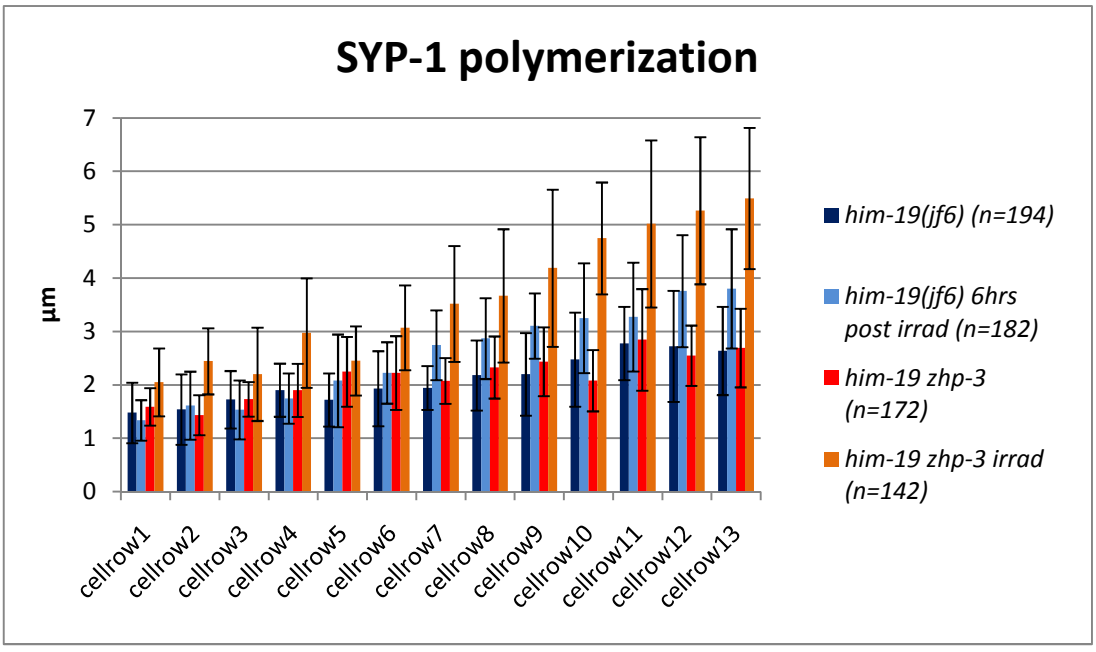

Figure 3.9 SYP-1 stretch-lengths in µm (y-axis) measured over the first 13 cell-rows after SYP-1 polymerization (x-axis) in the *C.elegans* germ line. Single *him-19(jf6)* and double *him-19 zhp-3* mutant gonads were dissected 6 hours post irradiation. Pictures of stained gonads were used to calculate SYP-1 stretches in meiotic nuclei using Photoshop software measure tool.

The morphology of *him-19 zhp-3* gonads was identical to *him-19* single mutants lacking a defined TZ with half-moon shaped nuclei. SYP-1 started to polymerize along chromosomes in a distinct manner at cell-row 15-25 after the distal tip comparably to wild-type and mutant *him-19* germ-lines. In the germ-line of *him-19 zhp-3* I measured SYP-1 stretches of 1,6 (±0,3) µm at the first cell-row and 2,7 (±0,7) µm at the last cell-row compared to 1,5 (±0,6) µm and 2,3 (± 0,5) µm in the *him-19(jf6)* single mutant [see figure 3.9]. Only a marginal difference of ~0,1 µm between averaged SYP-1 stretch lengths of the first and the last measured cell-row was seen in comparison to those observed in *him-19(jf6)* nuclei, but the level of SYP-1 polymerization observed in the double mutant showed a similar loading pattern during the period of measurement.

Radiation-treatment led to a similar restoration of SYP-1 polymerization in *him-19 zhp-3* double mutants as observed in *him-19* single mutants. I measured SYP-1 stretches at the first cell-row with 2 (±0,6) µm and at the last cell-row with 5,5 (±1,3) µm compared to 1,3 (±0,4) µm and 3,8 (± 1,1) µm long SYP-1 stretches in *him-19(jf6)* single mutant nuclei. However, the scored SYP-1 lengths were constantly longer over the period of measurement compared to *him-19(jf6)* worms after irradiation.

Polymerization of SYP-1 was clearly restricted in the in *him-19 zhp-3* double mutants equally to *him-19(jf6)* worms. Interestingly, I observed a strong increase in SYP-1 polymerization upon irradiation which was even more pronounced than the increase seen in the *him-19* alone. Strikingly, artificially induced DSBs increased polymerization of SYP-1 even more extensively than in the *him-19* single mutant and showed more wild-type like kinetics. The kinetics of SYP-1 polymerization in irradiated *him-19 zhp-3* gonads define ZHP-3 as a repressor of SYP-1 polymerization.

How does defective homologous pairing affect SYP-1 polymerization in the *him-19 sun-1* mutant background?

In C.elegans meiosis the SUN-1/KASH-bridge connects chromosome ends through the NE to microtubules (Penkner, Tang et al. 2007; Penkner, Fridkin et al. 2009; Sato, Isaac et al. 2009). In vitro assays reinforced its function in chromosome motion (Malone, Misner et al. 2003; Penkner, Fridkin et al. 2009; Sato, Isaac et al. 2009; Baudrimont, Penkner et al. 2010) and it was concluded that kinetic forces in the cytoplasm trigger active movement of chromosomes via the SUN/KASH NE-bridges. This motion in turn is believed to promote homologous and prevent non-homologous pairing interactions between chromosomes.

The absence of a defined transition zone and the high level of non-homologous chromosome synapsis in late pachytene are characteristics shared by *mtf-1/sun-1(jf18)* and *him-19(jf6)* mutant worms. With the construction of the *him-19 sun-1* double mutant strain I wanted to assess whether chromosome movement per se exerted an influence on SYP-1 polymerization. The following graph displays the resulting measurement of anti-SYP-1 stained double mutant versus *him-19* single mutant gonads.

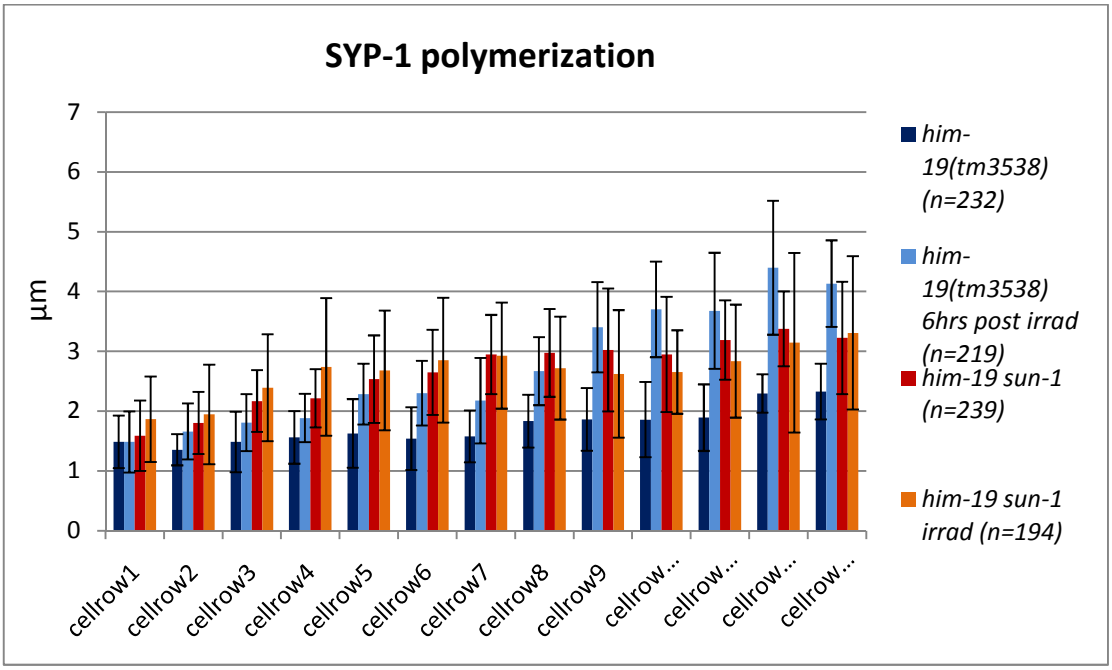

Figure 3.10 SYP-1 stretch-lengths in µm (y-axis) measured over the first 13 cell rows upon polymerization (x-axis) in the *C.elegans* germ line. Single *him-19* and double *him-19 sun-1* mutant gonads were prepared 6 hours after y-irradiation treatment. Pictures of stained gonads were used to score SYP-1 stretches in meiotic nuclei using Photoshop software measure tool.

Gonads of *him-19 sun-1* mutant worms displayed the same morphology as *him-19* single mutants lacking a defined TZ. The starting point of distinct SYP-1 polymerization was observed at the 13th-23th cell-row. Measured SYP-1 stretches the *him-19 sun-1* mutant background displayed a restricted loading of SYP-1. Even though the total SYP-1 stretch lengths [1,6 (±0,6) µm]in the first cell-row were on average 0,1 µm longer than in *him-19* worms [1,5 (±0,4) µm], the pattern of SYP-1 polymerization was comparable. I calculated 3,2 (±0,9) µm long SYP-1 stretches in nuclei of the last scored cell-row. Again the SYP-1 stretches were slightly longer compared to *him-19(tm3538)* [2,3 (±0,5) µm], but the localization pattern of SYP-1 observed over the period of measurement was similar.

After irradiation, the first measured cell-row was the 17th-25th and measured SYP-1 stretches were 1,9 (±0,7) µm. Similarly, I measured a sum of 2,3 (±0,5) µm in *him-19(tm3538)* worms. Upon irradiation SYP-1 stretch lengths of the last scored cell-row increased up to 3,3 µm (±1,3) µm compared to 4,1 (±0,7) µm in the *him-19* single mutant.

These results show that SYP-1 polymerization occurred in a restricted manner in *him-19 sun-1* mutants and can not be augmented by irradiation-induced DSBs. We can conclude that chromosome movement has a positive influence on SYP-1 polymerization or that non-homologous synapsis exerts a negative effect on SYP-1 polymerization.

Assessing homologous pairing in the *him-19* mutant germ-line:

In the previous section I have described that gamma irradiation in *him-19* mutant gonads leads to an increase in SYP-1 polymerization. I therefore wanted to assess whether SYP-1 polymerization in this mutant would go in hand with an increase in homologous pairing. Nuclei migrate on row per hour in the *C.elegans* germ-line (Crittenden, Leonhard et al. 2006). If irradiation would lead to an increase in pairing we should detect a cluster of nuclei with higher pairing values than in the unirradiated gonads.

Homologous pairing in *him-19* mutants bearing the *tm3538* allele was assessed by FISH assays using labeled 5S rDNA-probes that hybridize to chromosome V at the right arm, which is the same site were the PC is located (for details see “Materials and methods”).

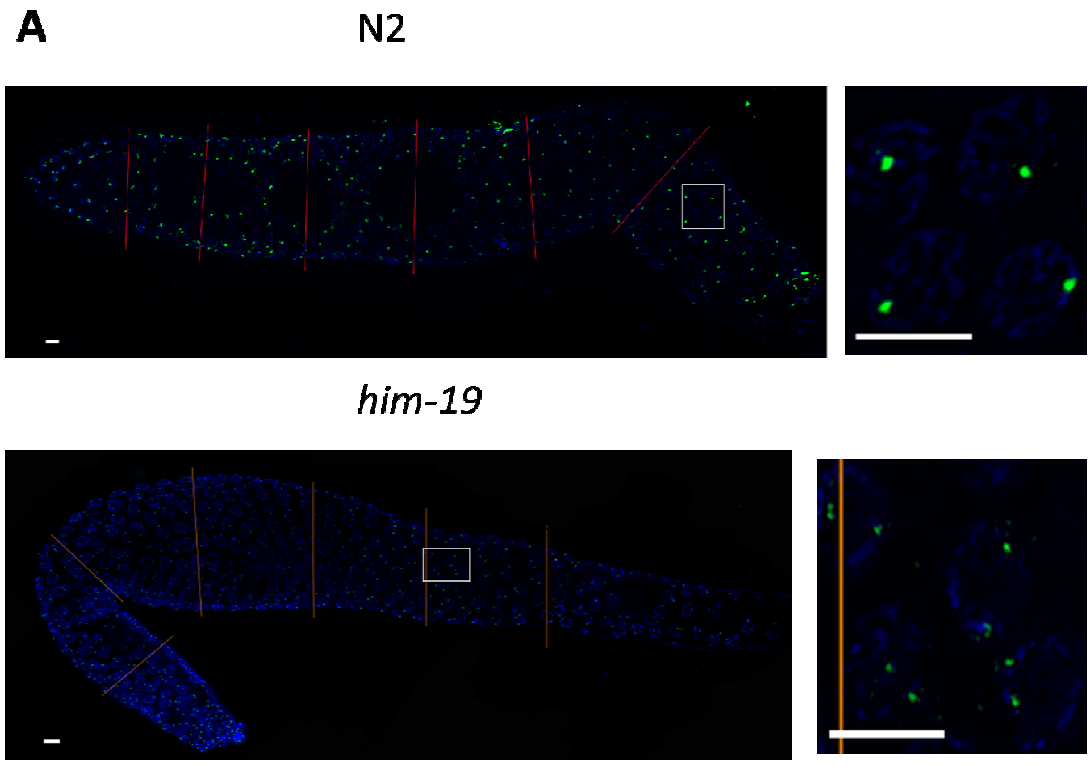

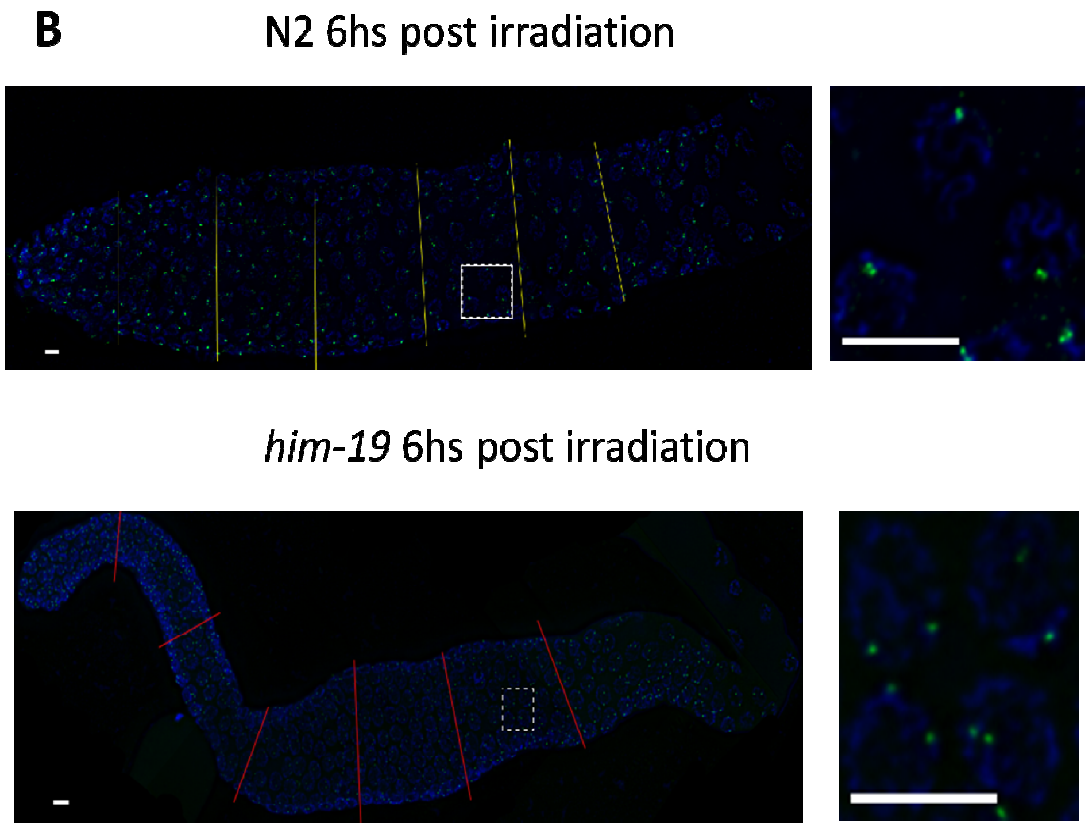

Figure 3.11 displays pictures of wild-type and *him-19(tm3538)* gonads (B) with and (A) without gamma-ray treatment taken at a magnification of 63x1 in oil. Chromatin is visualized by DAPI-staining and hybridized 5S rDNA at chromosome V appears as green signals. Pachytene cells are magnified for better visualization of nuclei and signals. Scale bars 5µm.

In the majority of wild-type pachytene nuclei chromosomes V appeared homologously paired indicated by a single signal per nucleus (see figure 3.11). In contrast homologous pairing of chromosome V was not observed in *him-19(tm3538)* mutant germ-lines demonstrated by mostly 2 signals per nucleus. To assess pairing levels gonads were divided into 7 zones of equal length and the percentage of paired 5S rDNA signals were scored (for details see “Materials and methods”). Results are represented in the following MSexel graph.

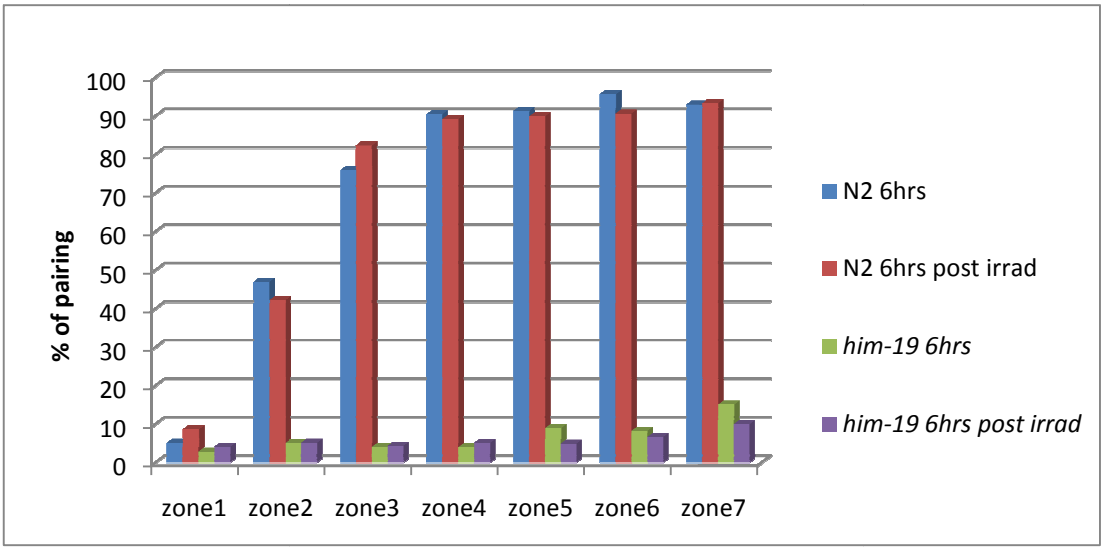

Figure 3.12 The graph shows the percentage of homologous pairing of chromosome V in wild-type (N2) and *him-19(tm3538)* mutant germ-lines with and without irradiation. The time point of gonad-preparation was 6 hours after irradiation. Gonads were divided into seven zones of equal length starting at the distal tip and ending at the beginning of diakinesis. The seven scored zones of gonads are shown at the y-axis and percentage of homologous pairing of chromosome V is represented at the x-axis. The FISH-signals were scored as a single signal when the distance between the signals was smaller than the size of the signals.

Constructed statistics (Figure 3.12) demonstrate that in zone 1, the mitotic zone, homologous pairing in wild-type gonads started with low background levels (~5%). The about 12 cell rows long transition zone was contained from the middle of zone 2 until the middle of zone 3. In this condensed chromatin structure homologous chromosome search takes place and homologous chromosome alignment follows indicated through ~45% of paired nuclei in zone 2. Homologous pairing levels at zone 3, where nuclei progress from TZ to early pachytene stage, represented ~75% and increased continuously at middle to late pachytene displaying 90% at zone 4/5 and 95% at zone 6. In zone 7 more than 90% of chromosomes were paired.

Homologous association of chromosome V remained steadily high and progressed continuously in wild-type germ lines 6 hours after irradiation. Only marginal differences of

about 5% were observed in zone 1-3 and 6 compared to the non-irradiated wild-type background.

Quantification of pairing in the mutant *him-19* background revealed that the pairing level in the mitotic zone was comparably low as in wild-type worms with 2% background level. Until zone 4 the pattern of homologous pairing remained steadily low with 3% and even at zone 5 and 6 never exceeded 9% indicating that chromosome V was unpaired in most nuclei. A maximum of pairing with 15% was detected at zone 7 corresponding to pachytene in the wild-type.

Analysis of meiotic nuclei in *him-19(tm3538)* worms dissected 6 hours post irradiation showed no noteworthy increase in homologous pairing of chromosome V compared to the non-irradiated gonads. Nuclei of gamma-radiation treated *him-19* mutant germ line never showed more than 9% homologous associations. Additionally, homologous pairing seemed to be slightly decreased in the irradiated wild type indicated through ~3% lower levels in the last 3 scored zones, which correspond to the pachytene stage.

To determine homologous pairing of chromosome V after a longer time period, FISH analysis was additionally carried out 24 hours post irradiation.

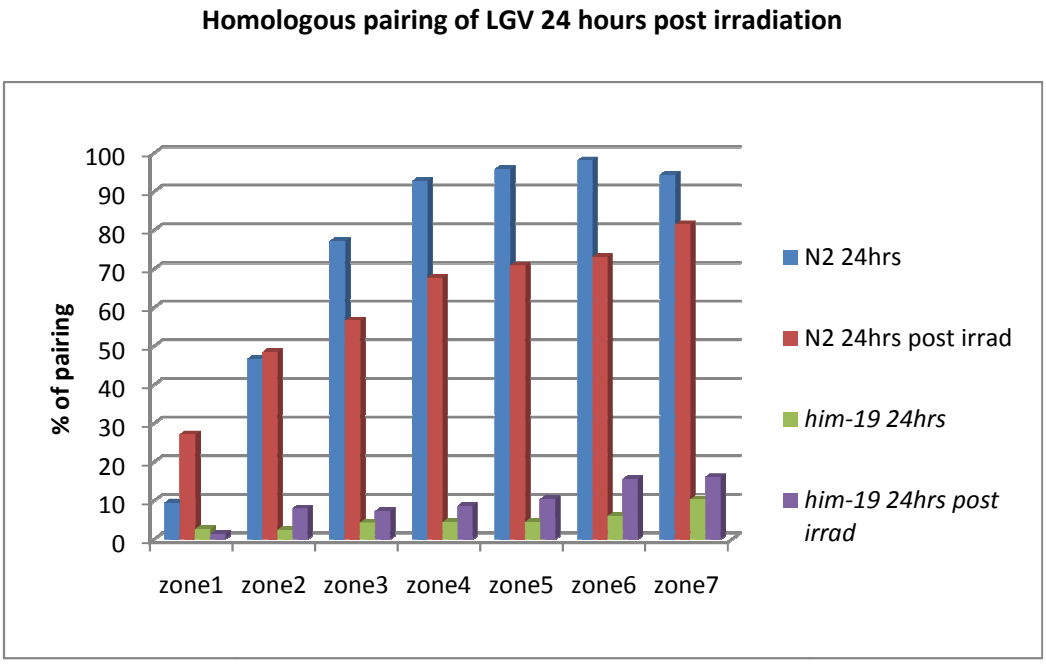

Figure 3.13 The diagram displays the percentages of homologous pairing of chromosome V in wild-type (N2) and *him-19(tm3538)* mutant gonads with and without irradiation treatment. The time point of gonad-preparation was 24 hours after irradiation. Gonads were divided into seven zones

of equal length starting at the distal tip and ending at the beginning of diakinesis. The seven scored zones of gonads are shown at the y-axis and percentage of homologous pairing of chromosome V is represented at the x-axis. The FISH-signals were scored as a single signal when the distance between the signals was smaller than the size of the signals themselves.

In the wild-type background homologous pairing of chromosome V was achieved in a similar manner at the later time point of gonad dissection (Figure 3.13). The background pairing level of mitotic zone 1 exhibited 8% which is comparable to earlier dissected germ-lines of wild-type worms. Likewise a continuously progression in homologous association was observed reaching 45% in zone 2 and 75% in zone 3. Most wild-type cells in zone 4-7 displayed homologously paired chromosome V signals evidenced by 90-98% of single FISH-signals.

Irradiation of wild-type worms affected homologous pairing in a promoting manner displayed by 26% in zone 1 which was fivefold the level of non-irradiated mitotic background. But in zone 2 of wild-type gonads observed level of homologous pairing appeared comparable to the non-irradiated background with 45%. During the pachytene stage, from zone 3 to 6, homologous associations increased continuously but remained steadily lower than in non-irradiated germ-lines (about 20%). Pairing of chromosome V displayed 15% lower levels at the last scored zone. However, irradiation-treatment seemed to affect proper pairing of chromosome V more extensively in wild-type worms 24 hours later.

Pairing frequency of chromosome V remained steadily low in *him-19* gonads dissected 54 hours post L4-selection (control of 24hours post irradiation) when compared to gonads dissected 18 hours earlier (control of 6hs post irradiation).

Slightly elevated pairing of chromosome V was observed in the *him-19* deficient background upon irradiation compared to the earlier non-irradiated time point. But even in zones displaying the highest value of homologous pairing (zone 6/7; see Figure 3.13), pairing levels never significantly exceeded the pairing levels observed in the mitotic region (only about 5%).

Taken together, both *him-19* mutant strains were shown to be defective in homologous pairing (Tang, Machacek et al. 2010). In contrast to SYP-1 polymerization, homologous

pairing was not increased upon irradiation in the absence of *him-19*. Therefore SYP-1 likely polymerized only along non-homologous chromosomes or individual chromosome axes. As expected, the two analyzed *him-19* mutant backgrounds were comparable with respect to homologous pairing of chromosome V.

Discussion:

The key tool for this work is the *him-19* mutant background allowing the analysis of meiotic DSB-dependent localization of the synaptonemal central element SYP-1. The extent of SYP-1 polymerization in *him-19* mutants with and without irradiation was investigated by Immunofluorescence and compared to the wild-type. Furthermore, the role of certain recombination intermediates in promoting SYP-1 polymerization in the absence of HIM-19 was assessed by constructing the double mutants and SYP-1 polymerization was compared upon irradiation. Finally I assessed whether the enhanced synapsis observed in *him-19* mutant worms was taking place between homologous chromosomes. To this end the level of chromosome pairing in *him-19* mutants in 6 and 24 hour time intervals after irradiation was scored throughout the meiotic time course applying FISH experiments.

Irradiation restores SYP-1 polymerization in the *him-19* mutant background

The two *him-19* mutant strains *tm3538* and *jf6* were analyzed and compared with respect to their viability and gonad morphology. The viability of the progeny in the *him-19(tm3538)* mutant background was comparable to that in *him-19(jf6)* over the reproductive time span. Additionally, gonads of both *him-19* mutant strains showed the same morphology as they lack the transition zone and univalents arise in diakinesis when chromatin was highlighted with DAPI. Interestingly, artificially induced DSBs restore SYP-1 polymerization onto chromatin in the absence of HIM-19. In contrast, the localization pattern of SYP-1 in wild-type gonads upon irradiation was comparably to non-irradiated gonads indicating that excessive desynapsis is not taking place upon irradiation. Hence, artificially induced DSBs do not affect SYP-1 polymerization in the wild-type background.

DSB repair and processing is required for SYP-1 polymerization in the absence of HIM-19

Gamma-irradiation induces more DSBs than would be by SPO-11 itself. In the absence of factors needed for DSB processing they cannot be repaired properly. As a consequence chromatin appears fragmented and clumped until late pachytene; repair via non

homologous end-joining (NHEJ) has been suggested to be responsible for the uncondensed and disorganized chromatin appearance (Hayashi, Chin et al. 2007). I found that SYP-1 polymerization in *him-19* was dependent on genes with a role in processing recombination intermediates (*mre-11, rad-51* and *msh-5*). In the double mutants I saw a clear restricted to absent polymerization upon irradiation. The marginal difference in SYP-1 stretch lengths might be contributed by the occurrence of highly unrepaired DSBs leading to fragmented chromatin in the absence of proper DSB repair and processing.

My results clearly connect DSB-induction and SYP-1 polymerization in the *him-19* deficient background; this in turn confirms the recently proposed cryptic DSB-dependent pathway in *C. elegans cra-1* mutants (Smolikov, Schild-Prufert et al. 2008). But in contrast to CRA-1, which has been reported to act downstream of SPO-11, HIM-19 function was proposed upstream of DSB-induction (Tang, Machacek et al. 2010). Nevertheless, the reported function of CRA-1 in regulating synapsis independently of homolog recognition, but dependent on DSB-induction, strongly resembles the situation in *him-19*. Thus, CRA-1 and HIM-19 seems to be involved in a cryptic DSB-dependent mechanism driving SC polymerization, which does not become apparent in a wild type worm under regular laboratory conditions. It might be worth the effort to reassess the completeness of SC polymerization in the *spo-11* or other crossover repair mutants.

Interestingly, y-irradiation induced DSBs restored SYP-1 polymerization in *him-19 zhp-3* double mutant gonads even more extensively than in *him-19(tm3538)* worms strongly resembling the polymerization pattern observed in irradiated wild-type gonads. Proper localization of ZHP-3 was proposed to be SC dependent (Jantsch, Pasierbek et al. 2004) and according to its localization pattern and genetic interactions ZHP-3 was suggested to act as a regulator of SC depolymerization (Bhalla, Wynne et al. 2008). In contrast, a clear activity of ZHP-3 in restricting SYP-1 polymerization was shown in this diploma thesis. Based on my data I propose that HIM-19 and ZHP-3 are both factors that contribute to DSB-dependent SYP-1 polymerization in *C.elegans* meiosis in a promoting and restricting way.

Chromosome movement promotes SYP-1 polymerization in *him-19* mutants

The local clustering of SUN-1 at chromosome ends was restored in the *him-19* mutant background upon irradiation, paralleled by chromatin clustering. In addition we showed that the SUN-1 aggregates were mobile (Penkner, Fridkin et al. 2009; Baudrimont, Penkner et al. 2010). However with my work I showed that the mere mobility of chromosome ends does not suffice to have pairing take place between homologous chromosomes. Moreover I wanted to assess whether the restored re-localization of SUN-1 aggregates at chromosome ends itself triggered chromosomal association of SYP-1 in worms lacking HIM-19. SYP-1 staining appeared restricted compared to wild-type and remained steady low after gamma-ray treatment in *him-19 sun-1* double mutants. When chromosomes do not move the chance to find a partner –homolog or non-homolog- decreases and as a consequence the rate of SYP-1 polymerization is also impeded. Given that I showed synapsis stabilizes non-homologous interactions in *him-19* mutants, I suggest that the residual observed SYP-1 polymerization takes place between non-homologous chromosomes or onto individual chromosome axes which found each other randomly in the absence of SUN-1 and HIM-19. In summary, my results indicate that chromosomes movement does not affect SYP-1 polymerization upon artificially DSBs induction when *him-19* is defective.

Homologous pairing is not restored upon irradiation in HIM-19 deficient worms

To assess whether SYP-1 polymerization in the *him-19* mutant would go in hand with an increase in homologous pairing FISH assays were carried out with *him-19(tm3538)* gonads. If irradiation would lead to an increase in pairing we should detect a population of nuclei with higher values than the unirradiated gonads. In contrast to SYP-1 polymerization, homologous pairing was not increased upon irradiation in the absence of *him-19*. Neither 6 nor 24 hours post irradiation a cluster of homologously paired chromosomes was observed. Hence SYP-1 likely polymerized along non-homologous chromosomes or onto individual chromosome axes in *him-19* worms.

Synapsis is crucial in many sexual reproducing organisms for connecting homologous chromosomes together to support proper crossover recombination. Understanding the regulation of formation of this highly conserved structure in the nematode *C.elegans* might lead to novel insights that can be tested whether they also hold true in higher organisms, like humans. With this potential risk factors for aneuploidy can be identified.

Abbreviations:

CHJP	close, stable homolog juxtaposition
CO	crossover
DAPI	4',6-diamidino-2-phenylindole
ddH_2O	double-distilled water
(ss)DNA	(single-stranded) Deoxyribonucleic acid
dNTP´s	Deoxynucleotide Triphosphate
DSB(s)	DNA double-strand break(s)
FISH	fluorescence In situ hybridization
Gy	gray = 1 J/kg = 100 rad
(d)HJ	(double) Holliday junction
hrs	hours
IF	immunofluorescence
kDa	kilo Dalton (= a unit of molecular mass equal to 1000 daltons; average MW of an amino acid = 110 daltons)
L4	larval stage 4 of *C.elegans* worms
M	molar (1 M = 1 mol/L)
mM	millimolar (1 mM = 10^{-3} mol/L)
min	minutes
µm	micrometers
NE	nuclear envelope
nm	nanometers
PC	pairing centers (= Homology recognition region/HRR)
POF	premature ovarian failure
rad	unit of absorbed radiation dose, 1 rad = 0.01 J/kg
SC	synaptonemal complex
SEI	single end invasion
TZ	transition zone
WT	wild-type

References:

Alpi, A., P. Pasierbek, et al. (2003). "Genetic and cytological characterization of the recombination protein RAD-51 in Caenorhabditis elegans." Chromosoma **112**(1): 6-16.

Antoshechkin, I. and P. W. Sternberg (2007). "The versatile worm: genetic and genomic resources for Caenorhabditis elegans research." Nat Rev Genet **8**(7): 518-532.

Baudrimont, A., A. Penkner, et al. (2010). "Leptotene/zygotene chromosome movement via the SUN/KASH protein bridge in Caenorhabditis elegans." PLoS Genet **6**(11): e1001219.

Bergerat, A., B. de Massy, et al. (1997). "An atypical topoisomerase II from Archaea with implications for meiotic recombination." Nature **386**(6623): 414-417.

Bhalla, N. and A. F. Dernburg (2008). "Prelude to a division." Annu Rev Cell Dev Biol **24**: 397-424.

Bhalla, N., D. J. Wynne, et al. (2008). "ZHP-3 acts at crossovers to couple meiotic recombination with synaptonemal complex disassembly and bivalent formation in C. elegans." PLoS Genet **4**(10): e1000235.

Borde, V. (2007). "The multiple roles of the Mre11 complex for meiotic recombination." Chromosome Res **15**(5): 551-563.

Borner, G. V., N. Kleckner, et al. (2004). "Crossover/noncrossover differentiation, synaptonemal complex formation, and regulatory surveillance at the leptotene/zygotene transition of meiosis." Cell **117**(1): 29-45.

Brenner, S. (1974). "The genetics of Caenorhabditis elegans." Genetics **77**(1): 71-94.

Carlton, P. M., A. P. Farruggio, et al. (2006). "A link between meiotic prophase progression and crossover control." PLoS Genet **2**(2): e12.

Chin, G. M. and A. M. Villeneuve (2001). "C. elegans mre-11 is required for meiotic recombination and DNA repair but is dispensable for the meiotic G(2) DNA damage checkpoint." Genes Dev **15**(5): 522-534.

Colaiacovo, M. P. (2006). "The many facets of SC function during C. elegans meiosis." Chromosoma **115**(3): 195-211.

Colaiacovo, M. P., A. J. MacQueen, et al. (2003). "Synaptonemal complex assembly in C. elegans is dispensable for loading strand-exchange proteins but critical for proper completion of recombination." Dev Cell **5**(3): 463-474.

Couteau, F., K. Nabeshima, et al. (2004). "A component of C. elegans meiotic chromosome axes at the interface of homolog alignment, synapsis, nuclear reorganization, and recombination." Curr Biol **14**(7): 585-592.

Couteau, F. and M. Zetka (2005). "HTP-1 coordinates synaptonemal complex assembly with homolog alignment during meiosis in C. elegans." Genes Dev **19**(22): 2744-2756.

Crittenden, S. L., K. A. Leonhard, et al. (2006). "Cellular analyses of the mitotic region in the Caenorhabditis elegans adult germ line." Mol Biol Cell **17**(7): 3051-3061.

Cromie, G. A. and G. R. Smith (2007). "Branching out: meiotic recombination and its regulation." Trends Cell Biol **17**(9): 448-455.

Dernburg, A. F., K. McDonald, et al. (1998). "Meiotic recombination in C. elegans initiates by a conserved mechanism and is dispensable for homologous chromosome synapsis." Cell **94**(3): 387-398.

Di Giacomo, M., M. Barchi, et al. (2005). "Distinct DNA-damage-dependent and -independent responses drive the loss of oocytes in recombination-defective mouse mutants." Proc Natl Acad Sci U S A **102**(3): 737-742.

Fridkin, A., A. Penkner, et al. (2008). "SUN-domain and KASH-domain proteins during development, meiosis and disease." Cell Mol Life Sci.

Gerton, J. L. and R. S. Hawley (2005). "Homologous chromosome interactions in meiosis: diversity amidst conservation." Nat Rev Genet **6**(6): 477-487.

Goodyer, W., S. Kaitna, et al. (2008). "HTP-3 Links DSB Formation with Homolog Pairing and Crossing Over during C. elegans Meiosis." Dev Cell **14**(2): 263-274.

Hassold, T., H. Hall, et al. (2007). "The origin of human aneuploidy: where we have been, where we are going." Hum Mol Genet **16 Spec No. 2**: R203-208.

Hassold, T. and P. Hunt (2001). "To err (meiotically) is human: the genesis of human aneuploidy." Nat Rev Genet **2**(4): 280-291.

Hayashi, M., G. M. Chin, et al. (2007). "C. elegans Germ Cells Switch between Distinct Modes of Double-Strand Break Repair During Meiotic Prophase Progression." PLoS Genet **3**(11): e191.

Hodgkin, J., H. R. Horvitz, et al. (1979). "Nondisjunction Mutants of the Nematode CAENORHABDITIS ELEGANS." Genetics **91**(1): 67-94.

Jantsch, V., P. Pasierbek, et al. (2004). "Targeted gene knockout reveals a role in meiotic recombination for ZHP-3, a Zip3-related protein in Caenorhabditis elegans." Mol Cell Biol **24**(18): 7998-8006.

Keeney, S. (2001). "Mechanism and control of meiotic recombination initiation." Curr Top Dev Biol **52**: 1-53.

Keeney, S., C. N. Giroux, et al. (1997). "Meiosis-specific DNA double-strand breaks are catalyzed by Spo11, a member of a widely conserved protein family." Cell **88**(3): 375-384.

Kelly, K. O., A. F. Dernburg, et al. (2000). "Caenorhabditis elegans msh-5 is required for both normal and radiation-induced meiotic crossing over but not for completion of meiosis." Genetics **156**(2): 617-630.

MacQueen, A. J., M. P. Colaiacovo, et al. (2002). "Synapsis-dependent and -independent mechanisms stabilize homolog pairing during meiotic prophase in C. elegans." Genes Dev **16**(18): 2428-2442.

MacQueen, A. J., C. M. Phillips, et al. (2005). "Chromosome sites play dual roles to establish homologous synapsis during meiosis in C. elegans." Cell **123**(6): 1037-1050.

Malone, C. J., L. Misner, et al. (2003). "The C. elegans hook protein, ZYG-12, mediates the essential attachment between the centrosome and nucleus." Cell **115**(7): 825-836.

Mandon-Pepin, B., P. Touraine, et al. (2008). "Genetic investigation of four meiotic genes in women with premature ovarian failure." Eur J Endocrinol **158**(1): 107-115.

Martinez-Perez, E. and A. M. Villeneuve (2005). "HTP-1-dependent constraints coordinate homolog pairing and synapsis and promote chiasma formation during C. elegans meiosis." Genes Dev **19**(22): 2727-2743.

Masson, J. Y. and S. C. West (2001). "The Rad51 and Dmc1 recombinases: a non-identical twin relationship." Trends Biochem Sci **26**(2): 131-136.

McKee, A. H. and N. Kleckner (1997). "A general method for identifying recessive diploid-specific mutations in Saccharomyces cerevisiae, its application to the isolation of mutants blocked at intermediate stages of meiotic prophase and characterization of a new gene SAE2." Genetics **146**(3): 797-816.

McKim, K. S., B. L. Green-Marroquin, et al. (1998). "Meiotic synapsis in the absence of recombination." Science **279**(5352): 876-878.

Nabeshima, K., A. M. Villeneuve, et al. (2005). "Crossing over is coupled to late meiotic prophase bivalent differentiation through asymmetric disassembly of the SC." J Cell Biol **168**(5): 683-689.

Nabeshima, K., A. M. Villeneuve, et al. (2004). "Chromosome-wide regulation of meiotic crossover formation in Caenorhabditis elegans requires properly assembled chromosome axes." Genetics **168**(3): 1275-1292.

Neale, M. J. and S. Keeney (2006). "Clarifying the mechanics of DNA strand exchange in meiotic recombination." Nature **442**(7099): 153-158.

Page, S. L. and R. S. Hawley (2004). "The genetics and molecular biology of the synaptonemal complex." Annu Rev Cell Dev Biol **20**: 525-558.

Pasierbek, P., M. Jantsch, et al. (2001). "A Caenorhabditis elegans cohesion protein with functions in meiotic chromosome pairing and disjunction." Genes Dev **15**(11): 1349-1360.
Penkner, A., Z. Portik-Dobos, et al. (2007). "A conserved function for a Caenorhabditis elegans Com1/Sae2/CtIP protein homolog in meiotic recombination." Embo J.
Penkner, A., L. Tang, et al. (2007). "The nuclear envelope protein Matefin/SUN-1 is required for homologous pairing in C. elegans meiosis." Dev Cell **12**(6): 873-885.
Penkner, A. M., A. Fridkin, et al. (2009). "Meiotic chromosome homology search involves modifications of the nuclear envelope protein Matefin/SUN-1." Cell **139**(5): 920-933.
Peoples-Holst, T. L. and S. M. Burgess (2005). "Multiple branches of the meiotic recombination pathway contribute independently to homolog pairing and stable juxtaposition during meiosis in budding yeast." Genes Dev **19**(7): 863-874.
Petronczki, M., M. F. Siomos, et al. (2003). "Un menage a quatre: the molecular biology of chromosome segregation in meiosis." Cell **112**(4): 423-440.
Prinz, S., A. Amon, et al. (1997). "Isolation of COM1, a new gene required to complete meiotic double-strand break-induced recombination in Saccharomyces cerevisiae." Genetics **146**(3): 781-795.
Rinaldo, C., P. Bazzicalupo, et al. (2002). "Roles for Caenorhabditis elegans rad-51 in meiosis and in resistance to ionizing radiation during development." Genetics **160**(2): 471-479.
Roeder, G. S. (1997). "Meiotic chromosomes: it takes two to tango." Genes Dev **11**(20): 2600-2621.
Sato, A., B. Isaac, et al. (2009). "Cytoskeletal forces span the nuclear envelope to coordinate meiotic chromosome pairing and synapsis." Cell **139**(5): 907-919.
Scherthan, H. (2007). "Telomere attachment and clustering during meiosis." Cell Mol Life Sci **64**(2): 117-124.
Severson, A. F., L. Ling, et al. (2009). "The axial element protein HTP-3 promotes cohesin loading and meiotic axis assembly in C. elegans to implement the meiotic program of chromosome segregation." Genes Dev **23**(15): 1763-1778.
Shinohara, A., H. Ogawa, et al. (1993). "Cloning of human, mouse and fission yeast recombination genes homologous to RAD51 and recA." Nat Genet **4**(3): 239-243.
Smolikov, S., A. Eizinger, et al. (2007). "SYP-3 restricts synaptonemal complex assembly to bridge paired chromosome axes during meiosis in Caenorhabditis elegans." Genetics **176**(4): 2015-2025.
Smolikov, S., K. Schild-Prufert, et al. (2008). "CRA-1 uncovers a double-strand break-dependent pathway promoting the assembly of central region proteins on chromosome axes during C. elegans meiosis." PLoS Genet **4**(6): e1000088.
Smolikov, S., K. Schild-Prufert, et al. (2009). "A yeast two-hybrid screen for SYP-3 interactors identifies SYP-4, a component required for synaptonemal complex assembly and chiasma formation in Caenorhabditis elegans meiosis." PLoS Genet **5**(10): e1000669.
Snowden, T., S. Acharya, et al. (2004). "hMSH4-hMSH5 recognizes Holliday Junctions and forms a meiosis-specific sliding clamp that embraces homologous chromosomes." Mol Cell **15**(3): 437-451.
Snowden, T., K. S. Shim, et al. (2008). "hMSH4-hMSH5 adenosine nucleotide processing and interactions with homologous recombination machinery." J Biol Chem **283**(1): 145-154.
Szostak, J. W., T. L. Orr-Weaver, et al. (1983). "The double-strand-break repair model for recombination." Cell **33**(1): 25-35.
Tang, L., T. Machacek, et al. (2010). "Mutations in Caenorhabditis elegans him-19 show meiotic defects that worsen with age." Mol Biol Cell **21**(6): 885-896.
Tzur, Y. B., K. L. Wilson, et al. (2006). "SUN-domain proteins: 'Velcro' that links the nucleoskeleton to the cytoskeleton." Nat Rev Mol Cell Biol **7**(10): 782-788.

Zetka, M. C., I. Kawasaki, et al. (1999). "Synapsis and chiasma formation in Caenorhabditis elegans require HIM-3, a meiotic chromosome core component that functions in chromosome segregation." Genes Dev **13**(17): 2258-2270.

Zickler, D. (1999). "[The synaptonemal complex: a structure necessary for pairing, recombination or organization of the meiotic chromosome?]." J Soc Biol **193**(1): 17-22.

Zickler, D. (2006). "From early homologue recognition to synaptonemal complex formation." Chromosoma **115**(3): 158-174.

Zickler, D. and N. Kleckner (1998). "The leptotene-zygotene transition of meiosis." Annu Rev Genet **32**: 619-697.

Curriculum vitae:

Personal information:

Name: Christina Wegrostek

Date of Birth: 04.05.1984

Gender: Female

Place of Birth: Vienna, Austria

Citizenship: Austrian

Marital Status: Single

Address: Krottenbachstrasse 245/4/1; 1190-Vienna, Austria

Email: christina_wegrostek@gmx.at

Telephone: 0043/676-6965056

Education:

1990-1994	*Elementary school* in Vienna
1994-2002	*Grammar school* in Vienna (Languages: English, French and Latin)
Since Oct. 2002	*Diploma Studies in molecular biology* at the University of Vienna
	Practical experience:
	Institute of Medical Biochemistry, Division of Molecular Biology,
	Group Prof. Reinhold Hofbauer
	Institute of Chromosome Biology, Group Dr. Verena Jantsch-Plunger
	Institute of Chromosome Biology, Group Prof. Michael Jantsch
Since Sept. 2009	*Diploma thesis* at the Institute of Chromosome Biology:
	"Connecting double strand breaks and synaptonemal complex assembly in *C.elegans*." Supervisor Dr. Verena Jantsch-Plunger

Teaching experience:

May 2009	*Tutor* at practical course "Genetik und Molekularbiologie (für Lehramtskandidaten)", University of Vienna, Austria

Publications:

Mutations in *Caenorhabditis elegans him-19* show meiotic defects that worsen with age. Tang L, Machacek T, Mamnun YM, Penkner A, Gloggnitzer J, *Wegrostek C*, Konrat R, Jantsch MF, Loidl J, Jantsch V. Mol Biol Cell. 2010 Mar;21(6):885-96. Epub 2010 Jan 13.

Leptotene/zygotene chromosome movement via the SUN/KASH protein bridge in *Caenorhabditis elegans*. Baudrimont A, Penkner A, Woglar A, Machacek T, *Wegrostek C*, Gloggnitzer J, Fridkin A, Klein F, Gruenbaum Y, Pasierbek P, Jantsch V. PLoS Genetics 2010 Nov 24;6(11):e1001219.

Employment history:

1998-2001	Barkeeper and Service at "Segafredo" Café Vienna-1190, Sieveringerstrasse
2002-2003	Barkeeper, Service and Technical Support at "BigNet" Internet Café Vienna-1060, Theobaldgasse 1
2006	Barkeeper and Service at Restaurant "Da Giovanni" Vienna-1210, Russbergstrasse 76

Additional activities:

2004	Spanish-course at Institute of languages at University of Vienna

Acknowledgements:

I want express special gratitude to my supervisors, Thomas Machacek and Verena Jantsch, not only for given me the opportunity to work on this research project, but also for sharing their insights and helping me to find my way through my research. Moreover I want to thank Thomas for introducing me into the model-organism *C.elegans*, teaching me patiently all the different analysis methods and aiding in every aspect. Beside his great teaching-skills, he always managed to jolly me along and became a good friend as well.

Further I want to thank the (former) members of the *C.elegans* laboratory -Alexandra Penkner, Alexander Woglar, Anahita Daryabeigi, Antoine Baudrimont and Christian Pflügl- for their professional and emotional support provided generously. The team spirit and the engagement of every individual person created a friendly and stimulating atmosphere. I really enjoyed working, exchanging experiences and laughing daily.

I will miss you all.